

Universidade Federal de Juiz de Fora  
Programa de Pós-Graduação em Engenharia Elétrica  
Engenharia Elétrica

Yan Furtado Coutinho

**Resource Allocation and Finite Block Length Regime**

Juiz de Fora

2021

Yan Furtado Coutinho

## **Resource Allocation and Finite Block Length Regime**

Dissertação de mestrado apresentada ao Programa de Pós-Graduação em Engenharia Elétrica da Universidade Federal de Juiz de Fora, na área de concentração em sistemas eletrônicos, como requisito para obtenção do título de Mestre em Engenharia Elétrica.

Orientador: Moisés Vidal Ribeiro

Coorientador: Guilherme Ribeiro Colen

Juiz de Fora

2021

Ficha catalográfica elaborada através do Modelo Latex do CDC da UFJF com os dados fornecidos pelo(a) autor(a)

Coutinho, Yan Furtado.

Resource Allocation and Finite Block Length Regime / Yan Furtado Coutinho. – 2021.

65 f. : il.

Orientador: Moisés Vidal Ribeiro

Coorientador: Guilherme Ribeiro Colen

Dissertação de Mestrado – Universidade Federal de Juiz de Fora, Engenharia Elétrica. Programa de Pós-Graduação em Engenharia Elétrica, 2021.

1. Comunicação de dados via rede de energia elétrica. 2. Alocação de recursos. 3. Blocos de comprimento finito. 4. Probabilidade de erro de símbolo. I. Ribeiro, Moisés Vidal, orient. II. Colen, Guilherme Ribeiro, coorient. III. Título.

**Yan Furtado Coutinho**

**Resource Allocation and Finite Block Length Regime**

Dissertação de mestrado apresentada ao Programa de Pós-Graduação em Engenharia Elétrica da Universidade Federal de Juiz de Fora, na área de concentração em sistemas eletrônicos, como requisito para obtenção do título de Mestre em Engenharia Elétrica.

Aprovada em: 24 de março de 2021

**BANCA EXAMINADORA**



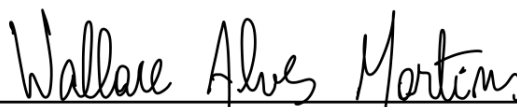
---

Professor Dr. Moisés Vidal Ribeiro - Orientador  
Universidade Federal de Juiz de Fora



---

Professor Dr. Guilherme Ribeiro Colen - Coorientador  
Centro de Instrução Almirante Wandenkolk



---

Professor Dr. Wallace Alves Martins  
Universidade Federal do Rio de Janeiro



---

Professor Dr. Alexandre Bessa dos Santos  
Universidade Federal de Juiz de Fora

*To my mother*  
*To my friends*  
*To my advisor*  
*To my colleagues*

## **ACKNOWLEDGMENTS**

First, I would like to thank God for guiding me through the most difficult times.

Secondly, I would like to thank my family, especially my mother Maria Angélica Furtado de Miranda, whose support and affection were and continue to be fundamental in this trajectory. Everything I am today is due to the structure provided by you with a lot of struggle and dedication. I also leave my gratitude to my friends for the moments of relaxation that are so necessary during this stage. My special thanks to Amanda Rodrigues de Melo for all the support and love she offered me along the way.

I would also like to thank my advisor, Professor Moisés Vidal Ribeiro, whose support and guidance contributed strongly not only to the writing of this work, but also to my professional and personal qualification. I thank Guilherme Ribeiro Colen for his teachings and research proposals. I am grateful for the advice and knowledge he gave me over this period.

Finally, I would like to thank all professors and employees of the Federal University of Juiz de Fora and my LCOM colleagues for contributing significantly to my academic and professional growth. I can't express enough how much you all helped me over those years.

“Thus, the task is not so much to see what no one yet has seen, but to think what nobody yet has thought about that which everybody sees.”

Arthur Schopenhauer

## RESUMO

Essa dissertação tem como objetivo introduzir versões melhoradas da técnica *Temporal Compressive Resource Allocation*, a qual é utilizada para alocação de recursos (bits e potência de transmissão) em sistemas de comunicação de dados multiportadora para aplicação em comunicação via rede de energia elétrica e discutir o regime de blocos de comprimento finito em sistemas de comunicação digital de dados monoportadora, quando o receptor não tem conhecimento da potência de transmissão e pode não conhecer o canal de comunicação. Nesse sentido, primeiramente é formulado o problema de alocação de recursos e é feita uma revisão da técnica original, ressaltando os pontos favoráveis da técnica e as melhorias sugeridas. As melhorias propostas são realizadas através da introdução de duas mudanças que aumentam a eficácia do processo de alocação de recursos quando a maximização da taxa de dados é almejada. A primeira mudança refere-se ao uso da razão sinal-ruído mínima de cada grupo de *microslots* para evitar picos na taxa de erro de símbolo em alguns *microslots* associados à componente fundamental nas redes de energia elétrica. A segunda mudança impõe o uso da matriz de razão sinal-ruído normalizada para estimar a correlação entre os *microslots*, uma vez que é considerado um parâmetro mais confiável para fornecer esse tipo de informação por ser resultado de menor processamento. Resultados numéricos, baseados em uma comparação entre a versão melhorada parcial, uma versão melhorada completa e a técnica original, mostram que ambas as versões aprimoradas são capazes de atender o limite superior da taxa de erro de símbolo com penalidade de perda de taxa de dados reduzida em comparação com a técnica original. Além disso, é possível perceber que o uso da matriz de razão sinal-ruído normalizada resulta em maior redução da complexidade computacional. Em seguida, é formulado o problema da transmissão de dados por blocos de comprimento finito em sistemas de comunicação digital de dados monoportadora em um cenário no qual o receptor deve estimar as potências de transmissão e do ruído aditivo considerando blocos de símbolos de comprimento finito, o que gera aleatoriedade no cálculo da razão sinal-ruído no receptor. Para contornar este problema, é proposto o uso de um fator de *gap* extra para minimizar o impacto de tal aleatoriedade e avaliar estatisticamente as consequências do uso de blocos de comprimento finito modelando uma variável aleatória quando são consideradas as constelações *M-QAM* e *M-PAM*. Análises numéricas mostram que, quando o receptor conhece o canal de comunicação, valores elevados do fator de *gap* extra são necessários para garantir a comunicação de dados confiável. Por outro lado, quando o canal de comunicação é desconhecido pelo receptor, blocos de comprimentos maiores ou maiores valores do fator de *gap* extra são cruciais para garantir a confiabilidade da comunicação de dados, especialmente na presença de um dispositivo malicioso, o qual é capaz de ouvir o sinal transmitido entre dois nós legítimos pertencentes à rede de dados.

Palavras-chave: Comunicação via rede de energia elétrica. Alocação de recursos. Blocos de comprimento finito. Probabilidade de erro de símbolo.



## ABSTRACT

This thesis aims to introduce enhanced versions of the Temporal Compressive Resource Allocation technique, which is used for resource allocation (bits and transmission power) in multi-carrier data communication systems for application in Power Line Communication and to discuss the finite block length regime in single-carrier digital data communication systems when the receiver is unaware of the transmission power and may be unaware of the communication channel. In this sense, the resource allocation problem is first formulated and a review of the original technique is shown, highlighting the favorable points of the technique and the possible suggested enhancements. Thus, the proposed enhancements are accomplished through the introduction of two changes that increase the effectiveness of the resource allocation process when the maximization of the data rate is desired. The first change refers to the use of the minimum signal-to-noise ratio of each set of microslots to avoid peaks in the symbol error rate in some microslots associated with the mains frequency in electrical power networks. The second change imposes the use of the normalized signal-to-noise ratio matrix to estimate the correlation between microslots since it is considered a more reliable parameter to provide this type of information because it is the result of less processing. Numerical results, based on a comparison between the partial enhanced version, a complete enhanced version, and the original technique, show that both enhanced versions are able to guarantee the symbol error rate upper bound with reduced data rate penalty compared to the original technique. In addition, it is possible to notice that the use of the normalized signal-to-noise ratio matrix results in a greater reduction in computational complexity. In the sequel, the problem of data transmission through blocks of finite length is formulated in single-carrier digital data communication systems in a scenario in which the receiver must estimate the transmission power and the additive noise power considering blocks of symbols of finite length, which generates randomness in the calculation of the signal-to-noise ratio at the receiver. To circumvent this problem, it is proposed the use of an extra gap factor to minimize the impact of such randomness and to statistically evaluate the consequences of using blocks of finite length by modeling a random variable when considering the  $M$ -QAM and  $M$ -PAM constellations. Numerical analyses show that when the receiver is aware of the communication channel, high values of the extra gap factor are necessary to ensure reliable data communication. On the other hand, when the communication channel is unknown by the receiver, blocks of greater lengths or greater values of the extra gap factor are crucial to ensure the reliability of data communication, especially in the presence of a malicious device, which is capable of overhearing the signal transmitted between two legitimate nodes that belong to the data network.

Key-words: Power Line Communication. Resource allocation. Finite block length. Symbol error probability.

## LIST OF FIGURES

Figure 1 – HS-OFDM mapping . . . . .	20
Figure 2 – Flowchart of the TCRA technique . . . . .	24
Figure 3 – The ETCRA technique. . . . .	29
Figure 4 – CCDF of data rate loss ratio . . . . .	31
Figure 5 – CCDF of computational complexity reduction ratio . . . . .	32
Figure 6 – SER per microslot . . . . .	32
Figure 7 – Block diagram of the single-carrier digital communication system . . . . .	35
Figure 8 – Relative frequency associated with the set of statistical distributions that best model $\beta$ considering $M$ -QAM constellations . . . . .	43
Figure 9 – Relative frequency associated with the set of statistical distributions that best model $\beta$ considering $M$ -PAM constellations . . . . .	44
Figure 10 – Block diagram of a wiretap channel model . . . . .	50
Figure 11 – Values of $F(a_{\text{QAM}}, k, \theta)$ when the receiver is aware of $h$ for (a) 4-QAM, (b) 16-QAM, and (c) 64-QAM constellations . . . . .	52
Figure 12 – Values of $F(a_{\text{PAM}}, \mu, \sigma)$ when the receiver is aware of $h$ for (a) 4-PAM, (b) 16-PAM, and (c) 64-PAM constellations . . . . .	53
Figure 13 – Values of $F(a_{\text{QAM}}, k, \theta)$ when the receiver is unaware of $h$ and $\Gamma_0 = 1$ dB for (a) 4-QAM, (b) 16-QAM, and (c) 64-QAM constellations . . . . .	55
Figure 14 – Values of $F(a_{\text{PAM}}, \mu, \sigma)$ when the receiver is unaware of $h$ and $\Gamma_0 = 1$ dB for (a) 4-PAM, (b) 16-PAM, and (c) 64-PAM constellations . . . . .	56

## LIST OF TABLES

Table 1 – Possible cases for resource allocation in the TCRA technique . . . . .	25
Table 2 – Values of $\rho_{A_i}[N]$ for the 16-QAM and 64-QAM constellations when a distribution other than the Gamma distribution is chosen as the best model for $\beta$ . . . . .	43
Table 3 – Values of $\rho_{A_i}[N]$ for the 4-PAM, 16-PAM, and 64-PAM constellations when a distribution other than the Lognormal distribution is chosen as the best model for $\beta$ . . . . .	45
Table 4 – Coefficients of the modeling function for the parameter $k$ of the Gamma distribution . . . . .	47
Table 5 – Coefficients of the modeling function for the parameter $\theta$ of the Gamma distribution . . . . .	47
Table 6 – Values of $k[N]$ achieved with its modeling function in comparison with the confidence interval of 95% for 4-QAM, 16-QAM, and 64-QAM constellations	47
Table 7 – Values of $\theta[N]$ achieved with its modeling function in comparison with the confidence interval of 95% for 4-QAM, 16-QAM, and 64-QAM constellations	48
Table 8 – Coefficients of the modeling function for the parameter $\mu$ of the Lognormal distribution . . . . .	49
Table 9 – Coefficients of the modeling function for the parameter $\sigma$ of the Lognormal distribution . . . . .	49
Table 10 – Values of $\mu[N]$ achieved with its modeling function in comparison with the confidence interval of 95% for 4-PAM, 16-PAM, and 64-PAM constellations	50
Table 11 – Values of $\sigma[N]$ achieved with its modeling function in comparison with the confidence interval of 95% for 4-PAM, 16-PAM, and 64-PAM constellations	51

## ACRONYMS

<b>AIC</b>	Akaike information criterion
<b>AWGN</b>	additive white Gaussian noise
<b>BEP</b>	bit error probability
<b>BIC</b>	Bayesian information criterion
<b>CCDF</b>	complementary cumulative distribution function
<b>CDF</b>	cumulative distribution function
<b>CIR</b>	channel impulse response
<b>CFR</b>	channel frequency response
<b>CSI</b>	channel state information
<b>DFT</b>	discrete Fourier transform
<b>DMT</b>	discrete multitone modulation
<b>ETCRA</b>	Enhanced Temporal Compressive Resource Allocation
<b>FBL</b>	finite block length
<b>HS-OFDM</b>	hermitian symmetric orthogonal frequency division multiplexing
<b>IBL</b>	infinite block length
<b>LPTV</b>	linear periodically time-variant
<b>LTI</b>	linear time-invariant
<b>nm-SNR</b>	multichannel normalized signal-to-noise ratio
<b>nSNR</b>	normalized signal-to-noise ratio
<b>IBL</b>	infinite block length
<b>IoT</b>	Internet of Things
<b>MLE</b>	Maximum Likelihood Estimation
<b>M-PAM</b>	$M$ -ary pulse amplitude modulation
<b>M-QAM</b>	$M$ -ary quadrature amplitude modulation
<b>OFDM</b>	orthogonal frequency division multiplexing
<b>PAM</b>	pulse amplitude modulation
<b>PDF</b>	probability density function
<b>PLC</b>	power line communication
<b>PLS</b>	physical layer security
<b>PSK</b>	phase-shift keying

<b>QAM</b>	quadrature amplitude modulation
<b>QoS</b>	quality of service
<b>r.v.</b>	random variable
<b>SC</b>	Smart Cities
<b>SCRA</b>	Spectral Compressive Resource Allocation
<b>SEP</b>	symbol error probability
<b>SER</b>	symbol error rate
<b>SG</b>	Smart Grids
<b>SH</b>	Smart Homes
<b>SNR</b>	signal-to-noise ratio
<b>STCRA</b>	Spectral-Temporal Compressive Resource Allocation
<b>TCRA</b>	Temporal Compressive Resource Allocation
<b>URLLC</b>	Ultra-reliable low-latency communication

## CONTENTS

<b>1</b>	<b>INTRODUCTION . . . . .</b>	<b>14</b>
1.1	OBJECTIVES . . . . .	16
1.2	THESIS ORGANIZATION . . . . .	17
1.3	SUMMARY . . . . .	17
<b>2</b>	<b>AN ENHANCED TEMPORAL COMPRESSIVE RESOURCE ALLO- CATION TECHNIQUE FOR PLC SYSTEMS . . . . .</b>	<b>18</b>
2.1	PROBLEM FORMULATION . . . . .	19
2.2	TEMPORAL COMPRESSIVE RESOURCE ALLOCATION TECHNIQUE REVIEW . . . . .	22
2.3	ENHANCED TEMPORAL COMPRESSIVE RESOURCE ALLOCATION TECHNIQUE . . . . .	25
2.4	NUMERICAL RESULTS . . . . .	30
2.5	SUMMARY . . . . .	33
<b>3</b>	<b>THE LACK OF TRANSMISSION POWER AND CHANNEL STATE INFORMATION KNOWLEDGE IN THE FINITE BLOCK LENGTH REGIME: A FIRST DISCUSSION . . . . .</b>	<b>34</b>
3.1	PROBLEM FORMULATION . . . . .	35
3.2	THE EXTRA GAP FACTOR . . . . .	37
3.3	DEDUCTIONS FOR <i>M</i> -QAM AND <i>M</i> -PAM CONSTELLATIONS . . . . .	39
3.3.1	<b>Square <i>M</i>-QAM Constellations . . . . .</b>	<b>39</b>
3.3.2	<b><i>M</i>-PAM Constellations . . . . .</b>	<b>40</b>
3.4	STATISTICAL MODELING . . . . .	41
3.4.1	<b><i>M</i>-QAM Constellations . . . . .</b>	<b>42</b>
3.4.2	<b><i>M</i>-PAM Constellations . . . . .</b>	<b>43</b>
3.4.3	<b>Similar Modeling Constellations . . . . .</b>	<b>44</b>
3.5	MODELING OF PARAMETERS OF THE CHOSEN DISTRIBUTIONS . . . . .	45
3.5.1	<b><i>M</i>-QAM Constellations . . . . .</b>	<b>45</b>
3.5.2	<b><i>M</i>-PAM Constellations . . . . .</b>	<b>47</b>
3.6	NUMERICAL ANALYSES . . . . .	49
3.6.1	<b>Case Study I . . . . .</b>	<b>51</b>
3.6.2	<b>Case Studies II and III . . . . .</b>	<b>52</b>
3.7	SUMMARY . . . . .	54
<b>4</b>	<b>CONCLUSION . . . . .</b>	<b>57</b>

4.1	FUTURE WORKS . . . . .	58
	<b>REFERENCES . . . . .</b>	<b>59</b>
	<b>APPENDIX A – Publications . . . . .</b>	<b>65</b>

## 1 INTRODUCTION

In recent years, especially in the last decade, the Internet of Things (IoT) concept has been growing in an overwhelming way, largely due to the development of telecommunications technologies related to Smart Grids (SG), Smart Homes (SH) and Industry 4.0 [1–3]. Nowadays, most electronic devices are interconnected with each other through data networks and even have the capability to operate only through sensor networks [4]. Thus, data communication between devices (for example, a sensor and a control center) is important for the smooth functioning of the system as a whole, mainly because most data networks operate with limited resources (hardware and energy) or with the most varied types of constraints (e.g., resource sharing, transmission power spectral density or frequency bandwidth).

In this sense, resource allocation has an important role in modern data communication systems since it allows to efficiently and effectively share the available channel resources. The resource allocation can be performed aiming to meet the requirements among multi-users and multi-servers demanding multi-services (e.g., real-time and non-real-time). On the other hand, the resource allocation can also be performed focusing on the demand of single-users for multi-services that, in the end, results in transmission power and bit allocation when a multi-carrier scheme is considered [5–9]. The resource allocation on a single-user scenario can be formulated based on two distinct criteria [10]: rate-adaptive, which aims to maximize the data rate given a maximum transmission power constraint, and margin-adaptive, which focus on minimizing the transmission power given a minimum data rate constraint. The so-called resources to be optimized for multi-carrier schemes based on orthogonal frequency division multiplexing (OFDM) can be considered, at a physical layer level, data rate [11, 12], transmission power [13–16], cyclic prefix length [17, 18], or even resources at a medium access control layer level [19–23], focusing on quality of service (QoS) and fairness among multiple users.

Regarding resource allocation in power line communication (PLC) systems, those based on microslots – which exploit the periodically time varying behavior of PLC channels – were first suggested in [24]. However, the resource allocation technique introduced in [24] is not feasible for real-time implementation due to the great computational complexity and the necessity of performing excessive data control exchanges among PLC devices. In order to circumvent those issues, [25] and [26] introduced low-cost resource allocation techniques that are called, respectively, Temporal Compressive Resource Allocation (TCRA) and Spectral Compressive Resource Allocation (SCRA). Both techniques exploit the periodically time varying characteristics of PLC channels with the advantage of offering a variable trade-off between performance and computational complexity. In [25], the existing relationships in the time-domain of PLC channels were taken into account to significantly reduce the computational complexity during the resource allocation process in exchange for small reductions in data rate, considering a dynamic resource allocation. Regarding [26], solutions were proposed for performing resource allocation by exploiting the existing correlation among the normalized signal-to-noise ratio (nSNR) associated



with consecutive subcarriers. Also, [26] introduced a solution for the combination of the SCRA and TCRA techniques, called Spectral-Temporal Compressive Resource Allocation (STCRA), in which existing relationships in time and frequency domains are jointly exploited. Those three techniques – TCRA, SCRA, and STCRA – result in suboptimal solutions that may be close to the optimum one, under constraint related to computational complexity and data rate.

Furthermore, it is important to emphasize that data exchanges through IoT devices can also be usually performed through intermittent exchanges of small packages (or blocks) of data and additional restrictions need to be applied to data communication systems, such as the need to transfer information with reduced latency [27, 28], a limitation in the transmission power [29] or even the need for a certain functionality at a physical layer level [30–32] to ensure the security of the transmitted information. Due to such circumstances, an increase in the number of works related to the data transmission through blocks of finite length has been observed since the well-established and fundamental communication theory does not cover these issues.

In fact, Shannon works thoroughly established that the theoretical channel capacity is the maximum rate at which the information can be reliably transmitted over a noisy channel, i.e., the maximum number of channel uses with an error probability reaching zero [33]. Despite being well-established, the concept of channel capacity developed by Shannon is based on the use of infinite length blocks and, in a scenario where the finite block length (FBL) regime is considered, it can no longer be enough for supporting the pursuit of reliable data communication systems since the achievable data rate is a more accurate parameter in such conditions. Regarding digital communication systems, bit error probability (BEP) and symbol error probability (SEP) suffer from the changes brought out by the FBL regime since the use of short-length blocks of data results in unpredictability related to the evaluation of error probabilities. For instance, tight expressions of achievable rate are introduced in [34, 35], which is a more suitable concept to be considered in the FBL regime when compared with the channel capacity. Following the same approach, [36] proposed a power allocation method aiming at the maximization of the achievable rate. The authors in [37] investigated the BEP of impulsive noise channels in a scenario of coded low-density parity-check and short-length blocks. Also, [38] addressed the issue of error probabilities evaluation with the FBL regime, where improved expressions for upper and lower bounds of the detection and decoding error probabilities were proposed. As mentioned, reduced latency and reliability of the data communication system are important features to be addressed when considering the data transmission through short-length blocks of data. In this sense, Ultra-reliable low-latency communication (URLLC) is also a recurrent subject of research in the FBL regime. In [39], a model for the block error rate was proposed, with the condition of perfect channel state information (CSI), based on the achievable rate of the system. Also, [40] investigated the optimization of both block length and pilot symbols length in a point-to-point URLLC system aiming at the maximization of throughput. Recently, some researches towards the FBL regime are being carried out in the field of secure data communications. In this sense, [41–43] addressed the issue of an achievable rate bound in

covert communications, i.e., the information exchange with a low probability of detection by a malicious entity. The data security in the FBL regime was also discussed at a physical layer level by [44], which contemplates the achievable security in short and finite-length blocks.

Regarding resource allocation (bit and power allocation) for single-user served by an OFDM scheme, several techniques have been introduced in order to present a feasible solution to the resource allocation problem in PLC systems [45–50]. Taking into account specifically the TCRA technique, it was noted that, despite all the important contributions showed in [25], the lack of a symbol error rate (SER) upper bound analysis to the technique is of most relevance since the violation of such constraint results in effective data rate losses, mostly caused by recurrently requested retransmissions. Therefore, the original TCRA technique needs to be investigated regarding a SER upper bound and, for means of comparison two enhanced versions are presented in this thesis, which are achieved based on two main modifications to the TCRA technique.

Also, in a scenario where the receiver is unaware of the transmission power, the FBL regime brings out unpredictability when designing data communication systems due to the fact that the receiver has to estimate the transmission power and the additive noise power in a scenario where the data transmission is performed through blocks of data with finite length. Therefore, it is notable the lack of researches considering the analysis of SEP in an uncoded digital data communication system in such conditions. With that in mind, the assumption of unawareness of transmission power with or without complete CSI deserves attention with the purpose of studying the impacts of the lack of such information when short and finite-length blocks of data are transmitted through data communication systems. Due to the randomness brought out by the FBL regime, a stochastic formulation needs to be considered, which leads to a statistical modeling methodology and, consequently, the discussion on the probability of the system to ensure a SEP when the FBL characteristics are considered in a typical data communication system between two nodes and under the presence of a malicious device that is capable of eavesdropping the information exchanged by other two legitimate nodes that belong to the data network.

## 1.1 OBJECTIVES

Given the aforementioned discussion and motivations regarding the single-user resource allocation and the FBL regime, the main objectives of the present thesis are summarized as follows:

- To introduce enhanced versions of the TCRA technique, called partial Enhanced Temporal Compressive Resource Allocation (ETCRA) and ETCRA, which are derived from two modifications to the original technique. Also, to compare, based on a data set composed of thousands of PLC channels estimates and additive noise measurements obtained from

a measurement campaign, the TCRA technique and the proposed enhanced versions. Such comparison analysis is achieved using data rate loss and computational complexity reduction ratios as performance evaluation criteria with the purpose of providing concrete results that the enhanced versions ensure the SER upper bound imposed into the PLC system based on the OFDM scheme while the TCRA technique violates such constraint.

- To investigate the distinct characteristics of the FBL regime and to analyze the probability of ensuring a target SEP designed for an uncoded single-carrier digital communication system impaired by additive white Gaussian noise (AWGN) when both the transmission power and the complete CSI are unknown by the receiver. Also, to present statistical modeling of the randomness brought out by the FBL regime and apply it to three distinct scenarios. The first and second scenarios are based on the data communication between transmitter and receiver, where the former considers the knowledge of the complete CSI by the receiver while the latter does not. The third case scenario takes place on a typical physical layer security (PLS) channel model, where a malicious device tries to overhear the information exchanged by two legitimate devices (nodes) of the data network.

## 1.2 THESIS ORGANIZATION

The remainder of this document is organized as follows:

- Chapter 2 introduces the two proposed modifications for the TCRA technique, which lead to the enhanced versions: partial ETCRA and ETCRA. The three techniques are compared considering both data rate loss and reduction of computational complexity, and it is shown that the enhanced versions are capable of ensuring the SER upper bound imposed into the data communication system.
- Chapter 3 describes the FBL regime and formulates in a stochastic manner the disparities brought out by the transmission of finite blocks of data. Based on the statistical modeling methodology presented in [51], numerical analyses are carried out in terms of the probabilities of ensuring a target SEP designed for the communication system in three distinct case scenarios.
- Chapter 4 places concluding remarks of this thesis and outlines future works.

## 1.3 SUMMARY

This chapter has presented a brief introduction of the thesis, addressing important concepts of resource allocation and discussing the characteristics of the FBL regime in digital communication systems. Also, the main objectives and the organization of this thesis have been summarized.

## 2 AN ENHANCED TEMPORAL COMPRESSIVE RESOURCE ALLOCATION TECHNIQUE FOR PLC SYSTEMS

PLC systems based on OFDM [52], similar to xDSL ones, operate in the baseband. It means that a baseband version of the OFDM scheme – hermitian symmetric orthogonal frequency division multiplexing (HS-OFDM) – with bit loading, which is commonly called discrete multitone modulation (DMT) [53–55], can be applied. In this scheme, the frequency domain representation of an OFDM symbol is mapped to exploit the hermitian symmetric property of the discrete Fourier transform (DFT) and to ensure that the corresponding time-domain representation of such a symbol is a real finite-length sequence that can be transmitted in the baseband. Thus, it is possible to take advantage of the characteristics of the OFDM scheme by applying the resource allocation process. Such process is performed based on the nSNR of each of the subcarriers, which can be obtained through the relationship between the squared magnitude of the channel frequency response (CFR) and the variance of the additive noise. Therefore, the nSNR is a parameter that represents the conditions of the communication medium to allow the estimation of energy and bits among the subcarriers. Usually, optimal resource allocation techniques tend to present high complexity and, consequently, are not feasible in real-time applications so that several suboptimal techniques are introduced in order to reduce such complexity. The TCRA technique offers a suboptimal solution to the resource allocation problem in exchange for reducing computational complexity [25]. However, despite the outstanding outcomes of the technique, the lack of a SER upper bound analysis lead to reduced effective data rate and, as a consequence, needs to be investigated. Based on the fact that single-user resource allocation is considered in this chapter, the term resource allocation from now on refers to bit and power allocation in an OFDM-based PLC system.

Aiming to address the aforementioned problem related to the TCRA technique, this chapter introduces and analyzes two main modifications to the technique. The first modification focuses on ensuring that the peak SER does not violate an imposed SER upper bound, while the second one contemplates the use of a distinct correlation coefficient within a cycle of the mains frequency in order to guarantee that the resource allocation process makes use of more reliable information. These modifications lead to two versions of the ETCRA technique. The first version, called partial ETCRA, utilizes only the modification regarding the assurance of a SER upper bound, maintaining the original correlation evaluation, while the second one, called ETCRA, applies both modifications.

This chapter is organized as follows: Section 2.1 presents the formulation of the resource allocation problem, in order to describe the data communication system in question. A review of the TCRA technique is made in Section 2.2. Section 2.3 describes the proposed ETCRA technique, as well as its mathematical formulation and introduces the proposed improvements over the TCRA technique. Section 2.4 presents the numerical results, assessing the performance of both TCRA and ETCRA techniques in terms of data rate and computational complexity.

Finally, Section 2.5 presents a succinct summary about this chapter.

## 2.1 PROBLEM FORMULATION

The TCRA technique introduced by [25] takes advantage of small differences among consecutive mains cycles, which is considered a quasi-linear periodically time-variant (LPTV) behavior of PLC channels. The quasi-LPTV assumption in TCRA [25] is a little different from the assumption of LPTV in [24]. In practice, the former assumption is much more realistic since the PLC channel can vary due to loads' dynamics. As a consequence, the assumption of quasi-LPTV behavior results in the violation of a SER upper bound in TCRA as well as in other techniques. In fact, the peaks on the SER related to the TCRA technique certainly result in the reduction of the effective data rate since retransmissions may be requested more often. Another source of data rate degradation in the use of TCRA concerns the way in which the channel correlation is evaluated, which relies on the use of multichannel normalized signal-to-noise ratio (nm-SNR) or data rate. The use of one of these parameters can result in loss of information<sup>1</sup>. However, such information is useful for efficiently characterizing the correlation between consecutive microslots, which is considered a relevant feature for performing resource allocation in PLC systems.

Thus, let us assume a baseband LPTV PLC channel with a coherence time  $T_c$  and a PLC system based on the HS-OFDM scheme. Also, microslots are defined in the time interval duration denoted by  $T_\gamma$ , such that the PLC channel is modeled as linear time-invariant (LTI) during these intervals since the constraint  $T_\gamma \ll T_c$  is fulfilled. For each cycle of the mains frequency,  $M$  microslots are defined. With that in mind, the vectorial representation of the channel impulse response (CIR) during the  $m^{\text{th}}$  microslot can be denoted by

$$\mathbf{h}_m = [h_m[0] \ h_m[1] \ \cdots \ h_m[L_{h_m} - 1]]^T, \quad (2.1)$$

in which  $L_{h_m}$  is the length of the CIR and  $(\cdot)^T$  denotes the transpose operator.

The HS-OFDM scheme is adopted in this work since the PLC system relies on the baseband data communication. Unlike a conventional OFDM symbol, which has  $N$  subcarriers, this scheme produces symbols of size  $2N$ , being composed of real and imaginary elements of the original OFDM symbol and operates in a frequency band from 0 to  $B$  Hz. In order to better clarify the HS-OFDM mapping, Figure 1 illustrates the procedure. Based on that,  $\mathbf{C} = [C_0 \ C_1 \ \cdots \ C_{N-1}]^T$  represents the OFDM symbol, in which the mapping will be applied. Thus,  $\mathbf{X} = [X_0 \ X_1 \ \cdots \ X_{2N-1}]^T$  denotes the vector after applying the mapping in  $\mathbf{C}$  and its  $k^{\text{th}}$

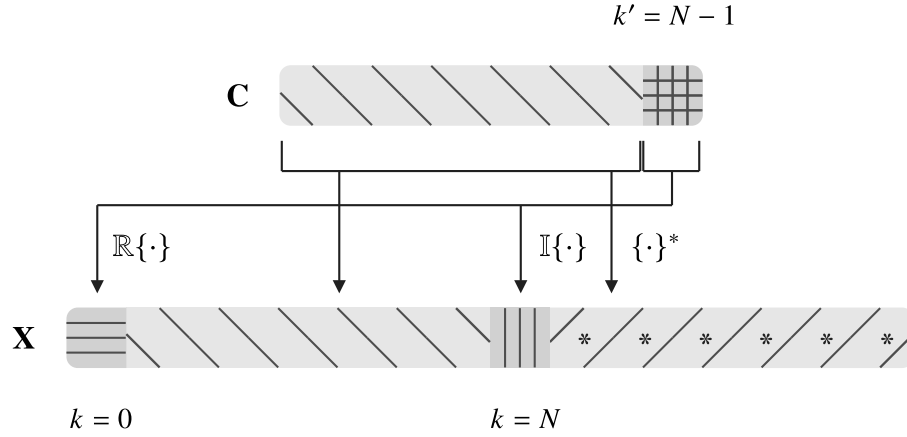
<sup>1</sup> According to data-processing inequality in the field of Information Theory, the processing of a data can reduce the amount of information associated with it.

element can be defined as

$$X_k = \begin{cases} \mathbb{R}\{C_{N-1}\} & , k = 0 \\ C_{k-1} & , k = 1, \dots, N-1 \\ \mathbb{I}\{C_{N-1}\} & , k = N \\ C_{2N-1-k}^* & , k = N+1, \dots, 2N-1 \end{cases}, \quad (2.2)$$

in which  $\mathbb{R}\{\cdot\}$  and  $\mathbb{I}\{\cdot\}$  are, respectively, the real and imaginary parts of a complex number and  $\{\cdot\}^*$  denotes the complex conjugate operator.

Figure 1 – HS-OFDM mapping



Source: Block diagram based on [10].

Thus, the DFT of the zero-padded version of the CIR at the  $m^{th}$  microslot is given by

$$\mathbf{H}_m = [H_m[0] H_m[1] \dots H_m[2N-1]]^T = \mathbf{W}_{2N} [\mathbf{h}_m^T \mathbf{0}_{2N-L_{hm}}^T]^T, \quad (2.3)$$

where  $\mathbf{W}_{2N} \in \mathbb{C}^{2N \times 2N}$  is the DFT matrix and  $\mathbf{0}_{2N-L_{hm}}$  is the  $(2N - L_{hm})$ -length column vector composed of zeros.

The noise is modeled as an additive stationary and colored Gaussian random process with frequency representation within the  $m^{th}$  microslot given by

$$\mathbf{V}_m = [V_m[0] V_m[1] \dots V_m[2N-1]]^T, \quad (2.4)$$

where  $V_m[k]$  is a random variable that models the additive noise at the  $m^{th}$  microslot and  $k^{th}$  subcarrier such that  $\mathbb{E}\{V_m[k]V_m[j]\} = \mathbb{E}\{V_m[k]\}\mathbb{E}\{V_m[j]\}$  for  $k \neq j$ ,  $\mathbb{E}\{V_m[k]\} = 0$  and  $\mathbb{E}\{\cdot\}$  denotes the expectation operator.

For the sake of simplicity, it can be defined

$$\mathbf{\Lambda}_{|H_m|^2} \triangleq \mathbf{diag} \left\{ |H_m[0]|^2 |H_m[1]|^2 \cdots |H_m[2N-1]|^2 \right\} \quad (2.5)$$

and

$$\mathbf{\Lambda}_{\sigma_{V_m}^2} \triangleq \mathbf{diag} \left\{ \sigma_{V_m[0]}^2 \sigma_{V_m[1]}^2 \cdots \sigma_{V_m[2N-1]}^2 \right\}, \quad (2.6)$$

in which  $\sigma_{V_m[k]}^2$  is the noise variance at the  $m^{th}$  microslot and  $k^{th}$  subcarrier, and  $\mathbf{diag}\{\cdot\}$  denotes a diagonal matrix. Based on that, the nSNR matrix, which represents the subcarrier signal-to-noise ratios (SNRs) when unit energy is applied to each subcarrier at the transmitter, is expressed as

$$\begin{aligned} \mathbf{\Lambda}_{\bar{\gamma}_m} &\triangleq \mathbf{diag} \left\{ \bar{\gamma}_m[0] \bar{\gamma}_m[1] \cdots \bar{\gamma}_m[2N-1] \right\} \\ &= \mathbf{\Lambda}_{|H_m|^2} \mathbf{\Lambda}_{\sigma_{V_m}^2}^{-1}, \end{aligned} \quad (2.7)$$

where the elements of the diagonal matrix  $\bar{\gamma}_m[k]$  represent the nSNR at the  $m^{th}$  microslot and  $k^{th}$  subcarrier.

As a consequence, based on [25], the nm-SNR at the  $m^{th}$  microslot is given by

$$\bar{\gamma}_m = \mathbf{det} \left( \mathbf{I}_{2N} + \mathbf{\Lambda}_{\bar{\gamma}_m} \right)^{\frac{1}{2N}} - 1, \quad (2.8)$$

where  $\mathbf{I}_{2N} \in \mathbb{R}^{2N \times 2N}$  and  $\mathbf{det}(\cdot)$  denote, respectively, the  $2N$ -size identity matrix and the determinant operator.

Taking into account the data communication in the baseband, the diagonal matrix of nSNR of size  $2N$  is characterized as double-sided. However, the resource allocation can be performed in an equivalent matrix of size  $N+1$ , denoted as one-sided, in order to reduce the computational complexity of the resource allocation algorithm. This procedure is described in [10] and, thus, the diagonal matrix of nSNRs containing the  $N+1$  subcarriers is represented as

$$\mathbf{\Lambda}_{\bar{\gamma}_m} \triangleq \mathbf{diag} \left\{ \bar{\gamma}_m[0] \bar{\gamma}_m[1] \cdots \bar{\gamma}_m[N] \right\}, \quad (2.9)$$

in which

$$\bar{\gamma}_m[k] = \begin{cases} \frac{|H_m[k]|^2}{\sigma_{V_m[k]}^2}, & k = 0, N \\ \frac{|H_m[k]|^2}{2\sigma_{V_m[k]}^2}, & k = 1, \dots, N-1 \end{cases}. \quad (2.10)$$

The resource allocation of a rate-adaptive problem during the  $m^{\text{th}}$  microslot can be represented by

$$\begin{cases} \left[ \Lambda_{b_m^o}, \Lambda_{E_m^o} \right] = f\left(\Lambda_{\bar{\gamma}_m}, E_t, \Gamma\right), & \text{if optimal allocation} \\ \left[ \Lambda_{b_m^o}, \Lambda_{E_m^o} \right] = f\left(\Lambda_{\bar{\gamma}_m}, E_t, \Gamma, \varphi\right), & \text{if suboptimal allocation} \end{cases}, \quad (2.11)$$

where  $f(\cdot)$  is the algorithm that performs the resource allocation, which is the water-filling algorithm in case of optimal allocation and a greedy rate-adaptive algorithm in case of suboptimal allocation [10];  $\Lambda_{b_m^o} = \mathbf{diag} \{b_m^o[0] b_m^o[1] \cdots b_m^o[N]\}$  is the matrix of bits allocated for performing data communication through the  $m^{\text{th}}$  microslot;  $\Lambda_{E_m^o} = \mathbf{diag} \{E_m^o[0] E_m^o[1] \cdots E_m^o[N]\}$  is the energy allocated to the  $m^{\text{th}}$  microslot;  $b_m^o[k]$  and  $E_m^o[k]$  are, respectively, the number of bits and the energy allocated at the  $m^{\text{th}}$  microslot and  $k^{\text{th}}$  subcarrier;  $E_t$  is the total energy to be shared among subcarriers;  $\Gamma \in \mathbb{R}_+$  is the gap factor from the Shannon capacity curve that defines a SER upper bound; and  $\varphi \in \mathbb{R}_+$  is the bit granularity for the resource allocation problem, i.e., the number of bits allocated in each iteration of the greedy algorithm.

Therefore, the data rate for the  $m^{\text{th}}$  microslot is denoted as

$$R_m^o = \frac{\text{Tr}(\Lambda_{b_m^o})}{T_{\text{sym}}}, \quad (2.12)$$

where  $\text{Tr}(\cdot)$  is the trace operator,  $T_{\text{sym}} = (2N + L_{cp})/F_s$  is the time duration of an HS-OFDM symbol,  $L_{cp}$  is the length of the cyclic prefix and  $F_s$  is the sampling frequency.

Thereby, the attained optimal data rate needs to be periodically updated and, as a consequence, computational complexity is significantly increased. However, according to [25], the existing relationship among successive cycles of the mains signal as well as inside each one of them in the time domain can be exploited for reducing the complexity associated with the resource allocation in OFDM-based PLC systems. In this sense, the TCRA technique was introduced in order to establish a trade-off between data rate and computational complexity, as detailed in Section 2.2.

## 2.2 TEMPORAL COMPRESSIVE RESOURCE ALLOCATION TECHNIQUE REVIEW

The TCRA technique considers the correlation of  $N_c \in \mathbb{N}$  cycles of the mains signal, each containing  $M$  microslots and divides the resource allocation problem into two stages. The first one is called Set Partitioning Procedure, which defines, based on the correlation evaluation, sets of microslots. The second stage is called Bit Loading Procedure, in which energy and bits are allocated between the microslots following the grouping defined in the previous stage. Both stages are presented below:

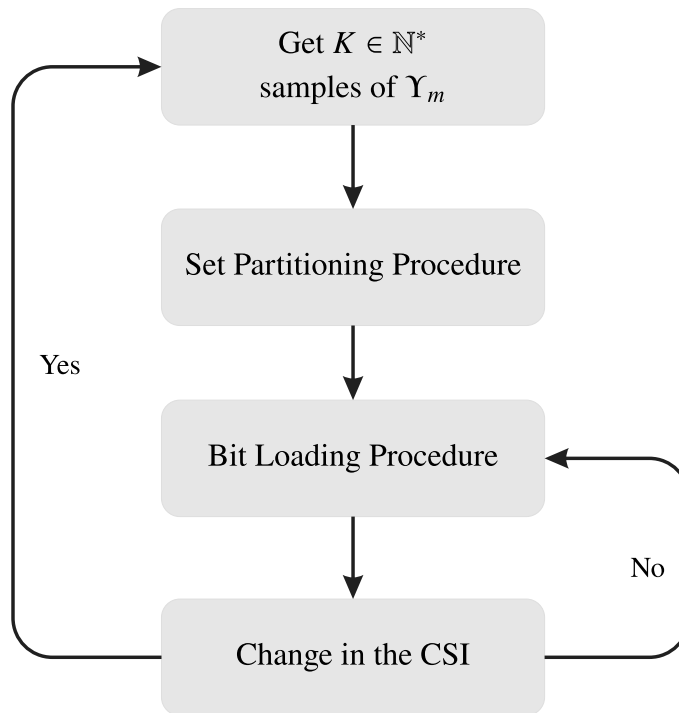


- **Set Partitioning Procedure:** at this stage the microslots are separated into groups, following the procedure below:
  - **Step #1:** Estimate the correlation  $C_{Y_m}[\tau] = \frac{\mathbb{E}\{(Y_m - \mu_Y)(Y_{m+\tau} - \mu_Y)\}}{\sigma_Y^2}$  using  $K \in \mathbb{N} \mid K \gg M$  samples of  $Y_m = R_m^o$  or  $Y_m = \bar{Y}_m$ .
  - **Step #2:** Evaluate the number of cycles of the mains signal with high correlation using  $N_c = \max_{C_{Y_m}[cM] \geq \alpha_2} \{c + 1\}$ , in which  $c = 0, 1, 2, \dots$ , is related to the  $c^{th}$  cycle and  $\alpha_2$  is the correlation threshold between  $N_c$  cycles of the mains.
  - **Step #3:** Define  $M$  sets composed of the positions of highly correlated microslots, i.e., microslots presenting  $C_{Y_m}[\tau] \geq \alpha_1$ . Mathematically,  $L_S^a = M$  sets are created, each one defined by  $S_l = \{l - 1 + \tau_1 + \tau_2 \mid C_{Y_m}[\tau_1] \geq \alpha_1, 0 \leq \tau_1 \leq M - 1, \tau_2 = cM, \text{ and } 0 \leq c \leq N_c - 1\}$ , in which  $l = 1, 2, \dots, L_S^a$  and  $\alpha_1$  is the correlation threshold within one cycle of the mains.
  - **Step #4:** Eliminate the sets possessing elements from other sets (e.g.  $S_l^b, L_S \leftarrow \min(L_S^a)$ , in which  $l = 1, 2, \dots, L_S$  and  $\min(\cdot)$  denotes the minimum operator, subject to  $\bigcup_{l=1}^{L_S} S_l^b = \{0, 1, \dots, MN_c - 1\}$ ). Note that  $S_l^b \cap S_i^b \neq \emptyset$ , where  $l \neq i \mid l, i \in \{1, 2, \dots, L_S\}$  can still occur.
  - **Step #5:** Define the data rate of a set as  $\epsilon_{S_l} = \min_j (Y_{S_l^b\{j\}})$ , where  $l = 1, 2, \dots, L_S$ ,  $j = 1, 2, \dots, L_{S_l}$ , and  $L_{S_l} = \text{card}(S_l)$ , in which  $\text{card}(S_l)$  is the cardinality of a set.
  - **Step #6:** Identify the sets associated with the microslots positions  $p$  within  $N_c$  cycles of the mains signal. Mathematically,  $l_p^* \triangleq \{l \mid S_l^b \cap \{p\} \neq \emptyset\}$ , in which  $0 \leq p \leq N_c M - 1$ .
  - **Step #7:** In order to eliminate intersections,  $L_S$  empty sets are defined,  $S_l = \emptyset$ ,  $1 \leq l \leq L_S$  and it is assumed that the microslot from the position  $p$  belongs only to the set  $S_{l_p^*\{q\}}$ , which possesses the higher data rate,  $q = \arg \max_j (\epsilon_{S_{l_p^*\{j\}}})$ , where  $1 \leq j \leq \text{card}(l_p^*)$ . Thus,  $S_l \cap S_i = \emptyset$  and  $\text{card}\left(\bigcup_{l=1}^{L_S} S_l\right) = MN_c$ .
- **Bit Loading Procedure:** at this stage, the bit and energy allocation is performed following the sets of microslots created in the Set Partitioning Procedure, as follows:
  - **Step #1:** Evaluate (2.11) and (2.12) for the first microslot of each set, i.e.,  $S_l\{1\}$ ,  $l = 1, 2, \dots, L_S$ .
  - **Step #2:** The resource allocation is applied for the remaining microslots of the sets defined by the Set Partitioning Procedure in the  $N_c$  cycles of the mains signal.

Figure 2 shows the flowchart for the TCRA technique. First,  $K$  samples from  $Y[m]$  are obtained so that the Set Partitioning Procedure and the Bit Loading Procedure are performed,

respectively. It is worth mentioning that if there is no change in CSI at the end of the process, only the Bit Loading Procedure will be executed, maintaining the grouping generated by the Set Partitioning Procedure. However, if there is a change in CSI,  $K$  new samples of  $\Upsilon[m]$  will be obtained and both procedures will be performed again.

Figure 2 – Flowchart of the TCRA technique



Source: Flowchart based on [25].

Moreover, since the PLC channel is considered quasi-LPTV, i.e., with small variations from one cycle to the other, three different cases are considered for the resource allocation problem, which are presented in Table 1 and described below:

- Case #1: the relationship between microslots within a cycle of the mains signal is explored for the purpose of resource allocation, being defined  $\alpha_1 < 1$  and  $\alpha_2 = 1$ .
- Case #2: the relationship between microslots belonging to distinct cycles of the mains signal is exploited, in which  $\alpha_1 = 1$  and  $\alpha_2 < 1$ .
- Case #3: the relationships between  $M$  microslots within a cycle and between the  $N_c$  cycles of the mains signal is investigated in order to reduce the computational complexity associated with the resource allocation process, defining  $\alpha_1 < 1$  and  $\alpha_2 < 1$ .

Despite the gains made by the TCRA technique by offering a trade-off between data rate and computational complexity, it is important to point out that due to the assumption of a quasi-LPTV behavior of the communication channel and, consequently, the use of the first microslot

Table 1 – Possible cases for resource allocation in the TCRA technique

Exploited Relationship	Case #1	Case #2	Case #3
Microslots within one cycle	×		×
Microslots from other cycles		×	×

Source: Personal collection.

within the set of microslots to perform the bit-loading to the remaining microslots of each set, the SER constraint may be violated since the channel conditions vary for each microslot of the cycle and between cycles, resulting in a reduced effective data rate, which definitely affects the overall performance of the data communication system. Another issue regards the use of  $\bar{\gamma}_m$  or  $R_m^o$  in order to evaluate the correlation among microslots. Such usage may represent a loss of important channel information since these parameters are outcomes of considerable processing.

To deal with the aforementioned problems, Section 2.3 introduces the modifications that lead to both partial ETCRA and ETCRA techniques, which ensure that the SER upper bound is totally satisfied during the resource allocation process applied to LPTV channels.

### 2.3 ENHANCED TEMPORAL COMPRESSIVE RESOURCE ALLOCATION TECHNIQUE

Given the presented characteristics of the TCRA technique and the issues addressed in the previous section, two main modifications are suggested with the purpose of ensuring an SER upper bound for the resource allocation problem and improving the evaluation of the correlation between microslots.

It is important to emphasize that for the TCRA technique, in [25] the PLC channel is considered quasi-LPTV, hence the argument of using several cases for grouping the microslots. However, as in [24, 56], in this chapter it is considered that the channel is invariant across consecutive cycles. Consequently, a different application of these cases must be considered. Case #1 can be normally applied. Case #2 has already a natural application since two consecutive mains cycles are identical. Therefore, there is no point in considering case #2 to analyze the reduction of computational complexity. Since case #3 is a combination of cases #1 and #2, it becomes senseless as well. Accordingly, the computational complexity reduction must be evaluated based only on case #1.

As [25] considered the PLC channel quasi-LPTV, during a real-time application, it is not possible to know perfectly the nSNR of all microslot for the current mains cycle or the following ones. As a consequence,  $\Lambda_{b_m}$  and  $\Lambda_{E_m}$  must be chosen based on the first microslot within the set of microslots, which are defined using the Set Partition Procedure and replicated on the remaining microslots belonging to the same set. This procedure is well discussed in

[25]. However, it is noted that such an approach may cause peaks on the SER associated with the remaining microslots belonging to the set, which can eventually violate the SER constraint applied to the resource allocation problem. Aiming to address this issue, the initial proposed enhancement focuses on the replacement of  $\Lambda_{b_m}$  and  $\Lambda_{E_m}$  associated with the first microslot of the set and the adoption of the worst nSNR for each subcarrier within the set of microslots instead. This is a conservative choice that ensures the non-violation of the SER constraint. The worst nSNR matrix related to the  $l^{th}$  set of microslots is expressed as

$$\mathbf{\Lambda}_{\Psi_l} = \mathbf{diag}\{\Psi_l[0] \Psi_l[1] \cdots \Psi_l[N]\}, \quad (2.13)$$

where  $\Psi_l[k]$  is the worst nSNR<sup>2</sup> associated with the  $k^{th}$  subchannel belonging to the  $l^{th}$  set of microslots. Note that

$$\Psi_l[k] = \min_j \bar{\gamma}_{S_l\{j\}}[k], \quad (2.14)$$

in which  $\min(\cdot)$  is the minimal operator,  $S_l$  denotes the group of microslots belonging to the  $l^{th}$  set,  $j \in \mathbb{N} \mid 1 \leq j \leq \text{card}(S_l)$  and  $\text{card}(\cdot)$  is the cardinality of a set. Therefore, the bit and energy allocation applied to all microslots of the  $l^{th}$  set is obtained by

$$\left[ \Lambda_{b_l}, \Lambda_{E_l} \right] = f\left(\mathbf{\Lambda}_{\Psi_l}, E_t, \Gamma, \varphi\right), \quad (2.15)$$

in which  $f(\cdot)$  defines the resource allocation technique using a greedy rate-adaptive algorithm.

Moreover, a modification is also introduced in the Set Partition Procedure. In [25], the correlation is evaluated using  $\bar{\gamma}_m$  or  $R_m^o$ , and the microslot with a correlation higher than a chosen threshold are grouped in the same set. However, this correlation does not efficiently exploit the richness of information associated with all subchannels since these parameters are outcomes of substantial processing. Therefore, it is proposed the replacement of  $\bar{\gamma}_m$  or  $R_m^o$  for  $\Lambda_{\bar{\gamma}_m}$  on the correlation evaluation since it carries much more information of all subchannels. The suggested parameter is denoted as  $\Lambda_{\bar{\gamma}_m}$  by reason of being much more representative for the current state conditions of the PLC channel in the  $m^{th}$  microslot. It is important to emphasize that, although the modified correlation evaluation has greater computational complexity, the Set Partitioning Procedure is applied only once, in case there is no change in the CSI during the Bit Loading Procedure, as explained in [25]. This implies that the complexity added by the modified correlation is minimal, compared to complexity additions to the Bit Loading Procedure, which is applied significantly more often in the resource allocation process. In this sense, the suggested

---

<sup>2</sup> The minimum operation is applied as a conservative approach for fulfilling a target SER and, as a consequence, some data rate reduction can be observed.

correlation coefficient can be evaluated as a normalized autocovariance of the nSNR matrix  $\Lambda_{\bar{\gamma}_m}$ , which is given by

$$\Phi(\tau) \triangleq \frac{\text{Tr}\left(\mathbb{E}\left\{\left(\Lambda_{\bar{\gamma}_m} - \Lambda_{\mu_{\bar{\gamma}_m}}\right) \odot \left(\Lambda_{\bar{\gamma}_{m+\tau}} - \Lambda_{\mu_{\bar{\gamma}_{m+\tau}}}\right)\right\}\right)}{\sqrt{\text{Tr}\left(\Lambda_{\sigma_{\bar{\gamma}_m}^2}\right)}\sqrt{\text{Tr}\left(\Lambda_{\sigma_{\bar{\gamma}_{m+\tau}}^2}\right)}}, \quad (2.16)$$

where  $\odot$  is the Hadamard product operator;  $\Lambda_{\mu_{\bar{\gamma}_m}} = \mathbb{E}\{\Lambda_{\bar{\gamma}_m}\}$  and  $\Lambda_{\mu_{\bar{\gamma}_{m+\tau}}} = \mathbb{E}\{\Lambda_{\bar{\gamma}_{m+\tau}}\}$ ;  $\Lambda_{\sigma_{\bar{\gamma}_m}^2} = \mathbf{diag}\{\sigma_{\bar{\gamma}_m}^2[0] \ \sigma_{\bar{\gamma}_m}^2[1] \ \cdots \ \sigma_{\bar{\gamma}_m}^2[N]\}$  and  $\Lambda_{\sigma_{\bar{\gamma}_{m+\tau}}^2} = \mathbf{diag}\{\sigma_{\bar{\gamma}_{m+\tau}}^2[0] \ \sigma_{\bar{\gamma}_{m+\tau}}^2[1] \ \cdots \ \sigma_{\bar{\gamma}_{m+\tau}}^2[N]\}$ , where  $\sigma_{\bar{\gamma}_m}^2[k]$  and  $\sigma_{\bar{\gamma}_{m+\tau}}^2[k]$  are, respectively, the variances of  $\bar{\gamma}_m[k]$  and  $\bar{\gamma}_{m+\tau}[k]$  at the  $k^{\text{th}}$  subcarrier;  $\tau \in \mathbb{Z} \mid 0 \leq \tau \leq M - 1$ ; and  $0 \leq \Phi(\tau) \leq 1$  since  $\Lambda_{\bar{\gamma}_m} \in \mathbb{R}_+^{(N+1) \times (N+1)}$  and  $\Lambda_{\bar{\gamma}_{m+\tau}} \in \mathbb{R}_+^{(N+1) \times (N+1)}$ .

In Figure 3, the algorithm related to the ETCRA technique is described and the steps for its implementation are detailed below:

- **Set Partitioning Procedure:**
  - **Step #1:** Evaluate (2.16).
  - **Step #2:** Define  $M$  sets composed of the positions of highly correlated microsloths. Mathematically,  $L_S^a = M$  sets are created, each one defined by  $\mathcal{S}_l = \{l - 1 + \tau \mid \Phi(\tau) \geq \alpha, 0 \leq \tau \leq M - 1\}$ , in which  $l = 1, 2, \dots, L_S^a$  and  $\alpha$  is the correlation threshold within one cycle of the mains.
  - **Step #3:** Eliminate the sets possessing elements from other sets (e.g.  $\mathcal{S}_l^b, L_S \leftarrow \min(L_S^a)$ , in which  $l = 1, 2, \dots, L_S$  and  $\min(\cdot)$  denotes the minimum operator, subject to  $\bigcup_{l=1}^{L_S} \mathcal{S}_l^b = \{0, 1, \dots, M - 1\}$ ). Note that  $\mathcal{S}_l^b \cap \mathcal{S}_i^b \neq \emptyset$ , where  $l \neq i \mid l, i \in \{1, 2, \dots, L_S\}$  can still occur.
  - **Step #4:** Define the data rate of a set as  $\epsilon_{\mathcal{S}_l} = \min_j(\bar{\gamma}_{\mathcal{S}_l^b\{j\}})$ , where  $l = 1, 2, \dots, L_S$ ,  $j = 1, 2, \dots, L_{\mathcal{S}_l}$ , and  $L_{\mathcal{S}_l} = \text{card}(\mathcal{S}_l)$ , in which  $\text{card}(\mathcal{S}_l)$  is the cardinality of a set.
  - **Step #5:** Identify the sets associated with the microsloths positions  $p$  within  $N_c$  cycles of the mains signal. Mathematically,  $l_p^* \triangleq \{l \mid \mathcal{S}_l^b \cap \{p\} \neq \emptyset\}$ , in which  $0 \leq p \leq M - 1$ .
  - **Step #6:** In order to eliminate intersections,  $L_S$  empty sets are defined,  $\mathcal{S}_l = \emptyset$ ,  $1 \leq l \leq L_S$  and it is assumed that the microslot from the position  $p$  belongs only to the set  $\mathcal{S}_{l_p^*\{q\}}$ , which possesses the higher data rate,  $q = \arg \max_j(\epsilon_{\mathcal{S}_{l_p^*\{j\}}})$ , where  $1 \leq j \leq \text{card}(l_p^*)$ . Thus,  $\mathcal{S}_l \cap \mathcal{S}_i = \emptyset$  and  $\text{card}\left(\bigcup_{l=1}^{L_S} \mathcal{S}_l\right) = M$ .
- **Bit Loading Procedure:**

- **Step #1:** Define for the  $l^{th}$  set of microslots and  $k^{th}$  subcarrier  $\Psi_{l,k} \mid 1 \leq l \leq L_S, 0 \leq k \leq N$ , with the purpose of applying the resource allocation.
- **Step #2:** Allocate  $\Lambda_{b_l}$  and  $\Lambda_{E_l}$  to the remaining microslots of each set.

The two aforementioned changes in the TCRA technique result in the so-called ETCRA. Based on [25], the steps for implementing ETCRA are detailed in Figure 3. However, a distinct approach can be implemented by considering only the modification displayed in (2.14) and disregarding the changes in the correlation addressed in the Step #1 of the Set Partitioning Procedure. For the sake of simplicity, this version of the technique is called partial ETCRA.

```

input :
 $\Lambda_{\bar{\gamma}_m}$  is the diagonal matrix of nSNRs for the Set Partitioning Procedure
 $M$  is the number of microslots within one cycle of the mains signal
 $\alpha \in \mathbb{R}$  is a threshold which determines the sets of microslots
 $E_t$  is the maximum energy to be distributed among microslots
 $\Gamma$  is the gap from the Shannon capacity curve
 $\varphi$  is the bit granularity of the resource allocation problem
output
:
 $\Lambda_{b_l}$  is the matrix corresponding to the number of bits allocated in each set of microslots
 $\Lambda_{E_l}$  is the matrix corresponding to the energy allocated in each set of microslots



---


begin
  while PLC system on do
    Set Partitioning Procedure
    - Step #1
    for  $\tau = 0$  to  $M - 1$  do
      
$$\Phi(\tau) \triangleq \frac{\text{Tr}\left(\mathbb{E}\left\{\left(\Lambda_{\bar{\gamma}_m} - \Lambda_{\mu_{\bar{\gamma}_m}}\right) \odot \left(\Lambda_{\bar{\gamma}_{m+\tau}} - \Lambda_{\mu_{\bar{\gamma}_{m+\tau}}}\right)\right\}\right)}{\sqrt{\text{Tr}\left(\Lambda_{\alpha^2_{\bar{\gamma}_m}}\right)}\sqrt{\text{Tr}\left(\Lambda_{\alpha^2_{\bar{\gamma}_{m+\tau}}}\right)}};$$

    end
    - Step #2
     $L_S^a = M;$ 
    for  $l = 1$  to  $L_S^a$  do
       $S_l^a = \{l - 1 + \tau \mid \Phi(\tau) \geq \alpha, 1 \leq l + \tau \leq M\};$ 
    end
    - Step #3
     $S_l^b, L_S \leftarrow \min L_S^a$ , in which
      
$$\bigcup_{l=1}^{L_S} S_l^b = \{0, 1, \dots, M - 1\};$$

    - Step #4
    for  $l = 1$  to  $L_S$  do
       $\epsilon_{S_l} = \min_j (\bar{\gamma}_{S_l^b(j)});$ 
       $S_l = \emptyset;$ 
    end
    - Step #5 and #6
    for  $p = 0$  to  $M - 1$  do
       $l_p^* = \{l \mid S_l^b \cap \{p\} \neq \emptyset\};$ 
       $q = \arg \max_j (\epsilon_{S_{l_p^*}^b(j)});$ 
       $S_{l_p^*}^b(q) = S_{l_p^*}^b(q) + \{p\};$ 
    end
    Bit Loading Procedure
    while CSI do not change do
      - Step #1
      for  $l = 1$  to  $L_S$  do
        for  $k = 0$  to  $N$  do
           $\Psi_l[k] = \min_j \bar{\gamma}_{S_l^b(j)}[k];$ 
        end
         $\Lambda_{\Psi_l} = \text{diag}\{\Psi_l[0] \Psi_l[1] \dots \Psi_l[N]\};$ 
         $[\Lambda_{b_l}, \Lambda_{E_l}] = f(\Lambda_{\Psi_l}, E_t, \Gamma, \varphi);$ 
      end
      - Step #2
      for  $l = 1$  to  $L_S$  do
        Apply  $\Lambda_{b_l}$  and  $\Lambda_{E_l}$  in other elements of  $S_l$ ;
      end
    end
  end
end

```

Figure 3 – The ETCRA technique.

## 2.4 NUMERICAL RESULTS

This section carries out a comparative study between TCRA, partial ETCRA, and ETCRA techniques based on a set of measured data. The data set is constituted by PLC channel estimates and additive noise measurements obtained from a measurement campaign carried out in seven residences in the city of Juiz de Fora, Brazil. The covered frequency band is between 1.7 and 100 MHz. Also, 232 measures were obtained with the use of the HS-OFDM scheme with  $N = 2048$  subchannels and a cyclic prefix of  $L_{cp} = 512$  samples, as described in [57]. The number of microslots during a time interval corresponding to one cycle of the mains signal is  $M = 32$  and the time interval of each microslot is equal to  $T_\gamma = (1/f_0)/M \approx 520 \mu\text{s}$ , where  $f_0 = 60$  Hz is the mains frequency. The value of  $M$  complies with the coherence time of the in-home PLC channel, see [57].

The performance comparisons are presented in terms of data rate loss ratio and computational complexity reduction ratio. The data rate loss ratio is expressed as

$$\eta = 1 - \frac{R_c}{R^o}, \quad (2.17)$$

where  $R^o$  denotes the data rate obtained by the greedy rate adaptive algorithm in all ( $M$ ) microslots using bit granularity  $\varphi = 2$  and  $R_c$  refers to the data rate obtained with TCRA, partial ETCRA or ETCRA.

On the other hand, the computational complexity reduction ratio is given by

$$\zeta = 1 - \frac{L_S}{M}, \quad (2.18)$$

in which  $L_S$  is the number of times TCRA, partial ETCRA, or ETCRA are applied during the resource allocation problem, whereas  $M$  is the total number of microslots used by the optimal resource allocation. Note that only case #1 was considered for the TCRA technique.

As in [25], the threshold  $\alpha$  defines the microslot grouping, following the rule that

$$\Phi(\tau) \geq \alpha, \quad (2.19)$$

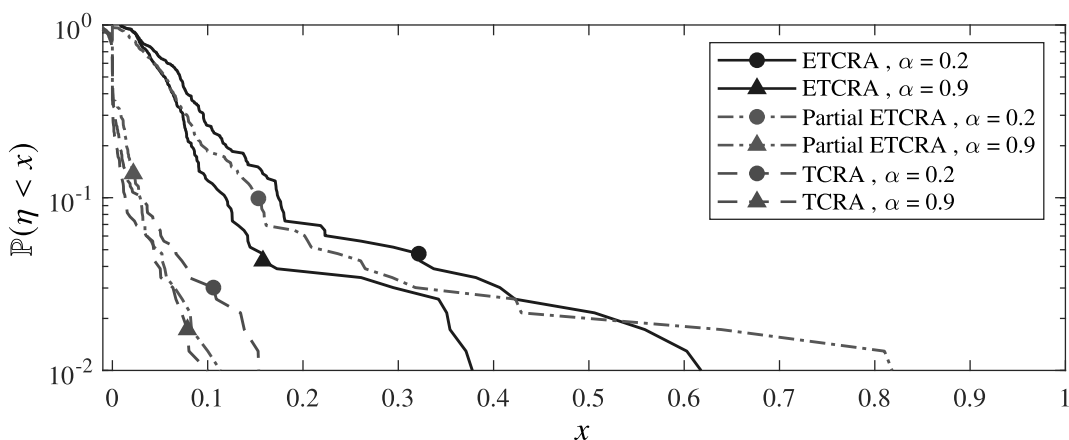
where  $\alpha \in \mathbb{R} \mid 0 \leq \alpha \leq 1$ . This parameter is adopted with the purpose of analyzing the impact of using different values for the correlation coefficient on the data rate loss ratio and the computational complexity reduction ratio. Note that  $\alpha = 0$  yields the grouping of all microslots in a single set (consequently,  $\zeta \approx 0.97$ ) while  $\alpha = 1$  implies the absence of grouping and, therefore, the creation of  $M$  sets in the Set Partitioning Procedure ( $\zeta = 0$ ).

First of all, let us analyze the complementary cumulative distribution function (CCDF) of the data rate loss ratio and computational complexity reduction ratio for the mentioned techniques. Figure 4 shows the CCDF of data rate loss ratio for  $\alpha = 0.2$  and  $\alpha = 0.9$ . Such



values of  $\alpha$  were chosen in order to better exemplify the implications of the variation of such parameter when values close to its extremes are taken into account. It is notable that, for all techniques, the variation of  $\alpha$  affects  $\eta$  directly. Higher values of  $\alpha$  imply a microslot grouping closer to its optimal and lower data rate loss. On the other hand, lower values of  $\alpha$  suggest the same allocation for all microslots and, consequently higher data rate loss, as illustrated in Figure 4. Note that ETCRA yields higher  $\eta$  than TCRA, which is an expected outcome given the modification presented in (2.14) being a trade-off between  $\eta$  and  $\zeta$  with a SER constraint guarantee. Considering the partial ETCRA, it is clear that this approach has intermediate performance between the two other techniques and, also, is more sensitive to variations in  $\alpha$ .

Figure 4 – CCDF of data rate loss ratio



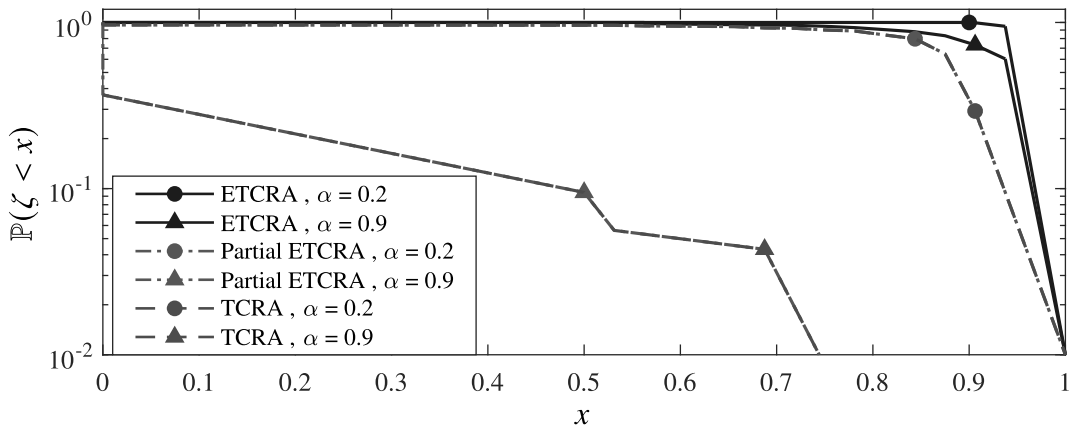
Source: Personal collection.

Regarding computational complexity, Figure 5 depicts a comparison between the three techniques by showing the CCDF of computational complexity reduction ratio for the same values of  $\alpha$  as in Figure 4. Perceive that ETCRA undergoes almost negligible changes in view of the variations in  $\alpha$ . TCRA and partial ETCRA, on the contrary, produces more distinct probabilities from each other regarding variations in  $\alpha$  (note that both curves are more distant from each other). Such a result showed in Figure 5 illustrates properly the trade-off offered by the ETCRA technique, where it yields higher data rate loss, however with a higher reduction to computational complexity. It also shows the computational complexity reduction yielded with the use of the modified correlation.

Finally, a discussion regarding SER is presented, which is the main focus of the modifications brought by the enhanced techniques. An SER upper bound is imposed on the system considering that the subchannel frequency bandwidth is substantially small, so that it can be assumed that each subchannel is impaired by AWGN and the channel attenuation is flat, as [10] thoroughly describes. This constraint is evaluated based on the gap from the Shannon capacity curve ( $\Gamma$ ) and can be expressed as

$$\xi_{\text{up}} = 4Q(\sqrt{3\Gamma}), \quad (2.20)$$

Figure 5 – CCDF of computational complexity reduction ratio

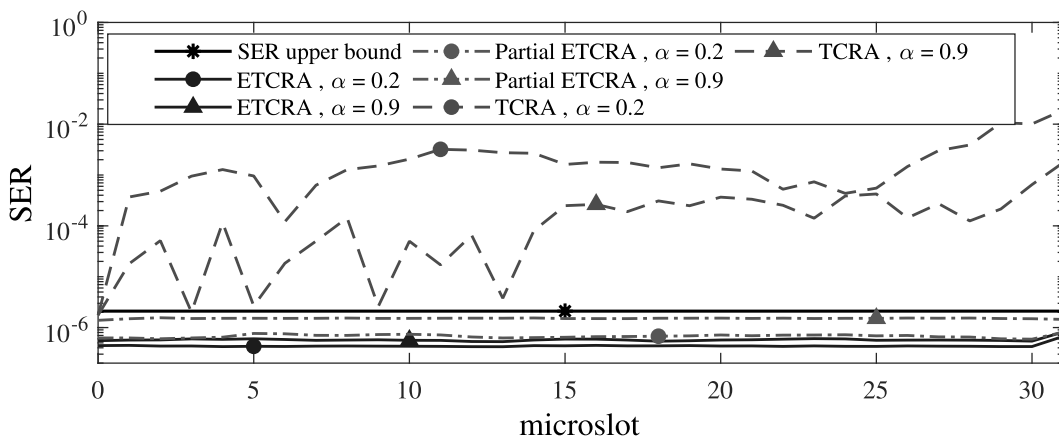


Source: Personal collection.

where  $Q(\cdot)$  is the tail distribution function of the standard normal distribution (i.e.,  $Q$ -function) and the gap is set as  $\Gamma = 9$  dB (resulting on  $\xi_{\text{up}} \approx 2.1 \times 10^{-6}$ ). Note that this constraint can be applied in every subchannel.

Thus, Figure 6 illustrates the simulated SER using quadrature amplitude modulation (QAM) schemes over an AWGN channel for all three techniques in comparison with the SER constraint defined by (2.20). Again, the chosen values of  $\alpha$  were the same as in Figure 4 and Figure 5. Note that, regardless of the chosen  $\alpha$ , both partial ETCRA and ETCRA achieve SER values lower than the predefined SER constraint for all microslots, with partial ETCRA being closer to the SER upper bound. On the other hand, TCRA violates the SER upper bound in most microslots for both values of  $\alpha$ .

Figure 6 – SER per microslot



Source: Personal collection.

## 2.5 SUMMARY

This chapter has introduced enhanced versions of the TCRA technique, which are called partial ETCRA and ETCRA. The proposed techniques, which are accomplished by introducing two modifications that increase the effectiveness of the resource allocation process based on rate adaptation, were presented by first reviewing the original technique and then focusing on the description of each enhancement. Also, numerical results were presented based on a comparative analysis between TCRA, partial ETCRA, and ETCRA. Such results showed that both enhanced versions are capable of fulfilling an SER upper bound with reduced data rate loss penalty in comparison to the original one.

### 3 THE LACK OF TRANSMISSION POWER AND CHANNEL STATE INFORMATION KNOWLEDGE IN THE FINITE BLOCK LENGTH REGIME: A FIRST DISCUSSION

Data communication through short and finite-length blocks has been drawing the attention of researchers in recent years, mainly due to the advance in the field of IoT, which cover SG, Smart Cities (SC) and Industry 4.0 demands [1–3], and the necessity of implementing multiple sensing systems [4] to fulfill the demand of modern technologies. Due to the characteristics of IoT sensing devices, such as the use of limited resources, and the transmission through short length blocks (or packets) of data, more requirements are imposed into the data communication systems, such as energy efficiency [29], the security of the transmitted information [31, 32, 58] and reduced latency of the data communication [59–61]. The FBL regime, i.e., the regime in which the data communication is performed through data blocks of finite length, offers several disparities regarding data communication features such as the channel capacity [34, 36] and error probabilities [37]. Shannon thoroughly established that the theoretical channel capacity is the maximum rate at which the information can be reliably transmitted over a noisy channel, i.e., the maximum number of channel uses with an error probability reaching zero. However, the concept of channel capacity introduced by Shannon is based on the use of infinite length blocks and, in a scenario where the FBL regime is considered, it can no longer be an accurate parameter for the data communication system. Likewise, BEP and SEP suffer from the changes brought out by the FBL regime since the use of short-length blocks results in unpredictability related to the evaluation of error probabilities.

Therefore, in this chapter, differently from the way the FBL regime is typically addressed in the literature, it is discussed the adoption of short and finite-length blocks in an uncoded digital communication system in which the transmission power and the knowledge of CSI are unknown by the receiver, and, as a consequence, each block can be seen as an occurrence of a finite-length random sequence. This scenario is adopted in view of highlighting the changes that occur in the SEP when finite length blocks are considered. With that purpose, the uncertainties due to the noise variance and constellation energy estimations by the receiver, brought out by the FBL regime, are summarized into a single random variable (r.v.). Consequently, the use of an extra gap factor in the SNR is proposed to overcome the additional randomness provoked by the FBL regime. By considering  $M$ -ary quadrature amplitude modulation ( $M$ -QAM) and  $M$ -ary pulse amplitude modulation ( $M$ -PAM) constellations, statistical models of such random variable are introduced when the length of the transmitted block ranges from 10 up to 1000 symbols.

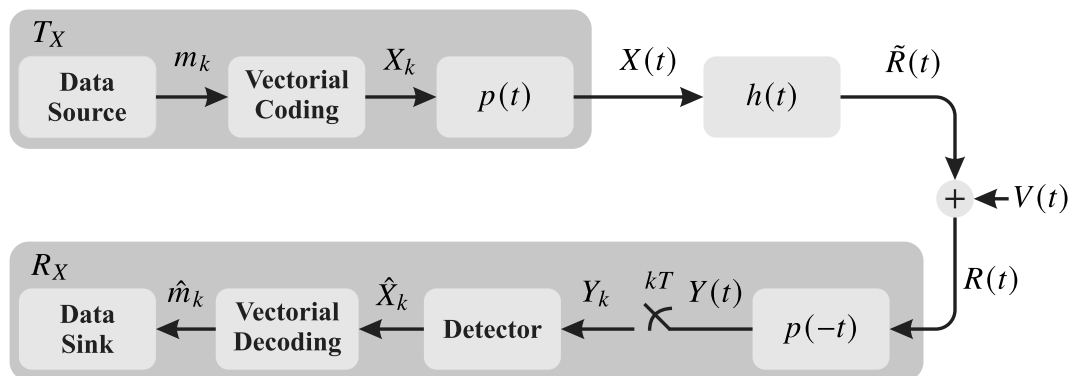
This chapter is organized as follows: Section 3.1 presents the formulation of the FBL regime problem, in order to describe the data communication system in question. Section 3.2 introduces the r.v. that models the randomness of the FBL regime as well as describes the proposed extra gap factor. Section 3.3 presents the deductions of the probabilities of ensuring an SEP upper bound for two distinct constellations. The statistical modeling of the r.v. is presented

in Section 3.4. Section 3.5 determines the modeling of the parameters of each chosen statistical distribution in function of the block length. Moreover, three distinct case scenarios are presented in Section 3.6 and a discussion is carried out based on the probabilities of ensuring SEP upper bounds. Section 3.7 addresses a brief summary on this chapter.

### 3.1 PROBLEM FORMULATION

Let us consider a data communication between two IoT devices as shown in Figure 7, where  $T_X$  and  $R_X$  represent the devices that transmit and receive data by using an uncoded single-carrier digital communication system. In this figure,  $m_k \in \{0, 1\}^b$  is the  $k^{\text{th}}$   $b$ -length binary and random message to be transmitted through this system;  $X_k \in \mathcal{X}$  is the symbol transmitted in the  $k^{\text{th}}$  symbol period;  $\mathcal{X} = \{x_0, x_1, \dots, x_{M-1}\}$  defines the constellation associated with an  $M$ -ary digital modulation scheme such that  $\text{card}(\mathcal{X}) = M$  is the cardinality of  $\mathcal{X}$  and  $b = \log_2 M$ ;  $p(t)$  is the squared root raised cosine pulse;  $X(t) = \sum_{k=-\infty}^{\infty} X_k p(t - kT)$  denotes the transmitted signal that is modeled as a stationary random process and  $T$  is the symbol period;  $h(t) = h\delta(t)$  models the CIR as a flat fading channel;  $R(t) = \tilde{R}(t) + V(t) = \sum_{k=-\infty}^{\infty} X_k p(t - kT) \star h(t) + V(t)$  denotes the received signal that is constituted by the summation of noise-free received signal  $\tilde{R}(t)$  and additive noise  $V(t)$ , which is modeled as a zero-mean white Gaussian random process, and  $\star$  is the convolution operator;  $Y(t) = \sum_{k=-\infty}^{\infty} X_k hq(t - kT) + p(-t) \star V(t)$  is the signal at the output of the matched filter and  $q(t) = p(t) \star p(-t)$  is the raised cosine pulse;  $Y_k = \tilde{R}_k + V_k = hX_k + V_k$  denotes the discrete-time version of the received signal with  $V_k \sim \mathcal{N}(0, \sigma_v^2)$ , i.e.,  $\mathbb{E}\{V_k\} = 0$  and  $\mathbb{E}\{|V_k|^2\} = \sigma_v^2$ ;  $\mathbb{E}\{V_k V_j^*\} = \mathbb{E}\{V_k\}\mathbb{E}\{V_j^*\} = 0, \forall k \neq j$ ;  $\mathbb{E}\{\cdot\}$  is the expectation operator,  $(\cdot)^*$  denotes the complex conjugate operator, and  $|\cdot|$  is the absolute value operator;  $\hat{X}_k$  and  $\hat{m}_k$  denote, respectively, the estimated symbol and message. Also, it is assumed perfect synchronization and the unawareness of the transmission energy by the receiver.

Figure 7 – Block diagram of the single-carrier digital communication system



Source: Personal collection.

Considering the transmission of infinite symbols, also called the infinite block length (IBL) regime, the target SEP ( $\mathcal{P}_{e,t}$ ) can be defined for the system, taking into account a specific

modulation scheme. Consequently, the required SNR at the receiver to achieve this SEP can be expressed as

$$\gamma_r = \frac{\mathcal{E}_x |h|^2}{\sigma_v^2}, \quad (3.1)$$

where  $\mathcal{E}_x = \mathbb{E}\{|X_k|^2\} = \frac{1}{M} \sum_{i=0}^{M-1} |x_i|^2$  is the average transmission energy which is equal to the average energy of the constellation. Note that it is assumed the knowledge of  $h$  and  $\sigma_v^2$  for the system design stage, which comes down to the evaluation of  $\mathcal{E}_x$  that satisfies  $\gamma_r$  and, consequently,  $\mathcal{P}_{e,t}$ .

However, in this work, the data communication among IoT devices is performed through the exchange of short-length blocks of data since these devices share limited amounts of information (e.g., temperature, status, blood pressure, etc.) and, accordingly, the FBL regime must be considered. In this scenario, the transmission occurs through short-length blocks of data containing a finite number ( $N$ ) of symbols, and, as a consequence, some distinct characteristics from the IBL regime arise. In fact, considering the FBL regime and the absence of information about transmission power and CSI, the receiver has to assume that the received symbols constitute an ergodic random process, and, as a consequence, information about the transmission power, the CSI and the additive noise must be estimated from a short-length block. As a matter of fact, each finite block of symbols can be treated as a subset of a random process derived from the IBL regime, which is now supposed to be an ergodic random process.

In this regard, let us consider that the  $p^{th}$  block composed of  $N$  random transmitted symbols is defined by  $X_{p,l} \in \mathcal{X}_p^N$ , with  $0 \leq l \leq N-1$ , and  $\mathcal{X}_p^N \subset \mathcal{X}$ . Consequently,  $\text{card}(\mathcal{X}_p^N) \leq \text{card}(\mathcal{X})$ . The channel is a block fading one and perfectly known by the receiver. Assuming that the receiver is capable of measuring the average energy of the transmitted symbols in the  $p^{th}$  block, then the average energy becomes an r.v. that is given by

$$\mathcal{E}_{x,\text{FBL}} = \frac{1}{N} \sum_{l=0}^{N-1} |X_{p,l}|^2, \quad (3.2)$$

where  $\mathcal{E}_{x,\text{FBL}}$  denotes the energy of the finite-length block. Note that  $\mathcal{E}_{x,\text{FBL}}$  is different for each block and, consequently, it can be considered an r.v.

Similarly, an  $N$ -length block constituted by consecutive samples of additive noise in the discrete-time domain is sensed by the receiver to measure its variance in the  $p^{th}$  block which can be given by

$$\sigma_{v,\text{FBL}}^2 = \frac{1}{N} \sum_{l=0}^{N-1} |V_{p,l} - V_{p,\text{avg}}|^2, \quad (3.3)$$

where  $\sigma_{v,\text{FBL}}^2$  is the noise variance of the finite-length block and  $V_{p,\text{avg}} = \frac{1}{N} \sum_{l=0}^{N-1} V_{p,l}$ . Note that for the FBL regime the noise random process with zero mean cannot be considered since the block has finite length.

Therefore, regarding the changes brought out by the FBL regime, it is pointed out that the SNR experienced by the receiver in the FBL regime is an r.v. that can be expressed as

$$\gamma_{\text{FBL}} = \frac{\mathcal{E}_{x,\text{FBL}} |h|^2}{\sigma_{v,\text{FBL}}^2}. \quad (3.4)$$

Note that, for this scenario,  $\mathcal{E}_{x,\text{FBL}}$  is defined for  $\mathcal{X}_p^N$  (a subset of  $\mathcal{X}$ ), diverging from  $\mathcal{E}_x$ . Also, when comparing (3.1) and (3.4),  $\gamma_{\text{FBL}} \neq \gamma_r$ . Due to this circumstance, the system design becomes imprecise and  $\mathcal{E}_x$  cannot be accurately determined to ensure the target SEP  $\mathcal{P}_{e,t}$  since  $\gamma_{\text{FBL}}$  is an r.v.

Hence, given the aforementioned formulation, Section 3.2 discusses the consequences brought out by the FBL regime into the described data communication system and presents the so-called extra gap factor for ensuring, with a certain probability, that the target SEP  $\mathcal{P}_{e,t}$  is satisfied.

### 3.2 THE EXTRA GAP FACTOR

In order to evaluate  $\mathcal{E}_x$  related to  $\mathcal{P}_{e,t}$  for the FBL regime, the r.v.s ( $\mathcal{E}_{x,\text{FBL}}$  and  $\sigma_{v,\text{FBL}}^2$ ) can be redefined with respect to their corresponding values in the IBL regime as follows:

$$\mathcal{E}_{x,\text{FBL}} \triangleq \beta_1 \mathcal{E}_x \quad (3.5)$$

and

$$\sigma_{v,\text{FBL}}^2 \triangleq \beta_2 \sigma_v^2, \quad (3.6)$$

where  $\beta_1$  is an r.v. that models the randomness imposed by the FBL regime regarding the average constellation energy and  $\beta_2$  is an r.v. associated with the randomness of the variance of the additive noise due to the use of the finite-length block (i.e., the FBL regime).

It is important to highlight that, according to the way the two variables are defined,  $\beta_1$  depends on the block length and the constellation associated with an  $M$ -ary digital modulation scheme (i.e.,  $\beta_1(N, \mathcal{X})$ ) while  $\beta_2$  is only dependent on the block length (i.e.,  $\beta_2(N)$ ). Also, note that both variables do not depend on the channel gain, which makes (3.5) and (3.6) valid for any LTI channel.

With that in mind,  $\gamma_{\text{FBL}}$  can be expressed in a distinct manner so that

$$\gamma_{\text{FBL}} = \frac{\beta_1 \mathcal{E}_x |h|^2}{\beta_2 \sigma_v^2} = \frac{\gamma_r}{\beta}, \quad (3.7)$$

where

$$\beta = \frac{\beta_2}{\beta_1} = \frac{\frac{\sigma_{v,\text{FBL}}^2}{\sigma_v^2}}{\frac{\mathcal{E}_{x,\text{FBL}}}{\mathcal{E}_x}}, \quad (3.8)$$

which is obtained by manipulating (3.5) and (3.6).  $\beta$  is an r.v. that models the randomness between  $\gamma_{\text{FBL}}$  (or SNR in the FBL regime) and  $\gamma_r$  (or the required SNR in the IBL regime). The importance of (3.7) is that all the randomness introduced by the FBL regime is concentrated in a single r.v., i.e.,  $\beta$ .

Ideally, in a scenario where infinite symbols are transmitted, the data communication system would be designed considering  $\mathcal{E}_x$ . However, in the FBL regime, due to the randomness of  $\gamma_{\text{FBL}}$ ,  $\mathcal{E}_x$  can no longer be accurately determined to thoroughly ensure  $\mathcal{P}_{e,t}$ . With that in mind, in order to ensure that  $\mathcal{P}_{e,t}$  is satisfied, an extra gap factor is introduced. With the addition of this parameter, the system is designed to present a distinct SNR at the receiver when compared to  $\gamma_r$ . The designed SNR can be defined as

$$\gamma_d \triangleq \Gamma_0 \gamma_{\text{FBL}} = \frac{\Gamma_0 \gamma_r}{\beta}, \quad (3.9)$$

where  $\Gamma_0$  denotes the extra gap factor.

Consequently, based on (3.9), the following theoretical conditions deserve attention:

- If  $\beta > \Gamma_0$ , then it can be concluded that

$$\gamma_d = \frac{\Gamma_0 \gamma_r}{\beta} < \gamma_r. \quad (3.10)$$

In other words, the system is designed with a lower SNR compared to  $\gamma_r$ . Consequently,  $\mathcal{P}_{e,t}$  is violated.

- If  $\beta \leq \Gamma_0$ , then the opposite conclusion is attained since

$$\gamma_d = \frac{\Gamma_0 \gamma_r}{\beta} \geq \gamma_r. \quad (3.11)$$

It means that, in this scenario, the system is being designed with a higher SNR in comparison with  $\gamma_r$  and, as a consequence,  $\mathcal{P}_{e,t}$  is satisfied.



This analysis presents an important outcome favoring the use of  $\Gamma_0$  to ensure  $\mathcal{P}_{e,t}$  when the FBL regime is considered in the system and the receiver is unaware of the transmission energy. Thus, based on the discussion presented in (3.10) and (3.11), the probability of ensuring that  $\mathcal{P}_{e,t}$  will be satisfied in the FBL regime can be expressed as

$$\mathbb{P}(\beta \leq \Gamma_0), \quad (3.12)$$

where  $\mathbb{P}(\cdot)$  denotes the probability operator. Note that such an outcome displayed by (3.12) is independent of  $\mathcal{P}_{e,t}$ , i.e., regardless of the value of  $\mathcal{P}_{e,t}$ , the probability of ensuring such value remains the same.

Lastly, since  $\Gamma_0$  is a parameter introduced into the system and established *a priori* in order to satisfy  $\mathcal{P}_{e,t}$ , the task of evaluating the probability given by (3.12) is summarized in determining a statistical distribution suitable for modeling the r.v.  $\beta$ . In this sense, the following sections carry out the discussion regarding the probabilities of ensuring SEP upper bounds for  $M$ -QAM and  $M$ -PAM constellations and the modeling of  $\beta$  for those cases considering the criteria used to evaluate the best statistical model for this variable.

### 3.3 DEDUCTIONS FOR $M$ -QAM AND $M$ -PAM CONSTELLATIONS

This section focuses on the deduction of the probabilities of ensuring SEP upper bounds of the square  $M$ -QAM and  $M$ -PAM constellations under the FBL regime detailed in Section 3.1.

#### 3.3.1 Square $M$ -QAM Constellations

First, the SEP for the  $M$ -QAM constellation in the FBL regime can be upper bounded [10, 62] by

$$\mathcal{P}_{e,\text{up,QAM,FBL}} = 4 \left( 1 - \frac{1}{\sqrt{M}} \right) \mathcal{Q} \left( \sqrt{\frac{3\gamma_d}{M-1}} \right) = 4 \left( 1 - \frac{1}{\sqrt{M}} \right) \mathcal{Q} \left( \sqrt{\frac{3\mathcal{E}_x \Gamma_0 |h|^2}{(M-1)\beta\sigma_v^2}} \right). \quad (3.13)$$

Also, for a SEP upper bound ( $\mathcal{P}_{e,\text{up,QAM}}$ ) and a given  $M$ -QAM constellation

$$\frac{d}{2\sigma_v} = K_{\text{QAM}}, \quad (3.14)$$

in which  $K_{\text{QAM}}$  ensures  $\mathcal{P}_{e,\text{up,QAM}}$ ,  $d$  denotes the minimal distance between two adjacent points in the  $M$ -QAM constellation.

Consequently, the probability that  $\mathcal{P}_{e,\text{up,QAM,FBL}}$  is lower than  $\mathcal{P}_{e,\text{up,QAM}}$  (i.e.,  $\mathbb{P}(\mathcal{P}_{e,\text{up,QAM,FBL}} \leq \mathcal{P}_{e,\text{up,QAM}})$ ) can be obtained if

$$\sqrt{\frac{3\mathcal{E}_x\Gamma_0|h|^2}{(M-1)\beta\sigma_v^2}} \geq K_{\text{QAM}}. \quad (3.15)$$

Evaluating (3.15), it can be concluded that

$$\beta \leq \frac{3\mathcal{E}_x\Gamma_0|h|^2}{(M-1)K_{\text{QAM}}^2\sigma_v^2} \quad (3.16)$$

ensures that  $\mathcal{P}_{e,\text{up,QAM,FBL}} \leq \mathcal{P}_{e,\text{up,QAM}}$ . Consequently, the value of  $\mathbb{P}(\mathcal{P}_{e,\text{up,QAM,FBL}} \leq \mathcal{P}_{e,\text{up,QAM}})$  can be expressed as

$$\mathbb{P}(\mathcal{P}_{e,\text{up,QAM,FBL}} \leq \mathcal{P}_{e,\text{up,QAM}}) = \int_0^{a_{\text{QAM}}} f_\beta(x) dx, \quad (3.17)$$

where  $f_\beta(x)$  is the probability density function (PDF) of the chosen statistical distribution for  $\beta$  and

$$a_{\text{QAM}} = \frac{3\mathcal{E}_x\Gamma_0|h|^2}{(M-1)K_{\text{QAM}}^2\sigma_v^2}. \quad (3.18)$$

Assuming that  $\beta$  is modeled by a Gamma distribution with shape  $k$  and scale  $\theta$  (i.e.,  $\beta \sim \Gamma(k, \theta)$ )<sup>1</sup>, then

$$\mathbb{P}(\mathcal{P}_{e,\text{up,QAM,FBL}} \leq \mathcal{P}_{e,\text{up,QAM}}) = F(a_{\text{QAM}}, k, \theta), \quad (3.19)$$

where  $F(a_{\text{QAM}}, k, \theta)$  is the cumulative distribution function (CDF) of the Gamma distribution at the corresponding point  $a_{\text{QAM}}$ .

### 3.3.2 $M$ -PAM Constellations

Considering  $M$ -PAM constellations, the SEP in the FBL regime can be upper bounded [10, 62] by

$$\mathcal{P}_{e,\text{up,PAM,FBL}} = 2\left(1 - \frac{1}{M}\right)\mathcal{Q}\left(\sqrt{\frac{3\gamma_d}{M^2-1}}\right) = 2\left(1 - \frac{1}{M}\right)\mathcal{Q}\left(\sqrt{\frac{3\mathcal{E}_x\Gamma_0|h|^2}{(M^2-1)\beta\sigma_v^2}}\right). \quad (3.20)$$

<sup>1</sup> The Gamma distribution is used since the statistical modeling in Section 3.4 shows that it is the best distribution to model  $\beta$  for  $M$ -QAM constellations.

Also, for a SEP upper bound ( $\mathcal{P}_{e,\text{up,PAM}}$ ) and an  $M$ -PAM constellation

$$\frac{d}{2\sigma_v} = K_{\text{PAM}}, \quad (3.21)$$

in which  $K_{\text{PAM}}$  ensures  $\mathcal{P}_{e,\text{up,PAM}}$ ,  $d$  denotes the minimal distance between two adjacent points in the  $M$ -PAM constellation.

Consequently, the probability that  $\mathcal{P}_{e,\text{up,PAM,FBL}}$  is lower than  $\mathcal{P}_{e,\text{up,PAM}}$  (i.e.,  $\mathbb{P}(\mathcal{P}_{e,\text{up,PAM,FBL}} \leq \mathcal{P}_{e,\text{up,PAM}})$ ) can be obtained if

$$\sqrt{\frac{3\mathcal{E}_x\Gamma_0|h|^2}{(M^2-1)\beta\sigma_v^2}} \geq K_{\text{PAM}}. \quad (3.22)$$

Evaluating (3.22), it can be concluded that

$$\beta \leq \frac{3\mathcal{E}_x\Gamma_0|h|^2}{(M^2-1)K_{\text{PAM}}^2\sigma_v^2} \quad (3.23)$$

ensures that  $\mathcal{P}_{e,\text{up,PAM,FBL}} \leq \mathcal{P}_{e,\text{up,PAM}}$ . Consequently, the value of  $\mathbb{P}(\mathcal{P}_{e,\text{up,PAM,FBL}} \leq \mathcal{P}_{e,\text{up,PAM}})$  can be expressed as

$$\mathbb{P}(\mathcal{P}_{e,\text{up,PAM,FBL}} \leq \mathcal{P}_{e,\text{up,PAM}}) = \int_0^{a_{\text{PAM}}} f_\beta(x) dx, \quad (3.24)$$

where  $f_\beta(x)$  is the PDF of the chosen statistical distribution for  $\beta$  and

$$a_{\text{PAM}} = \frac{3\mathcal{E}_x\Gamma_0|h|^2}{(M^2-1)K_{\text{PAM}}^2\sigma_v^2}. \quad (3.25)$$

Considering that  $\beta$  is modeled by a Lognormal distribution with mean  $\mu$  and standard deviation  $\sigma$  (i.e.,  $\ln(\beta) \sim \mathcal{N}(\mu, \sigma)^2$ ), then

$$\mathbb{P}(\mathcal{P}_{e,\text{up,PAM,FBL}} \leq \mathcal{P}_{e,\text{up,PAM}}) = F(a_{\text{PAM}}, \mu, \sigma), \quad (3.26)$$

where  $F(a_{\text{PAM}}, \mu, \sigma)$  is the CDF of the Lognormal distribution at the corresponding point  $a_{\text{PAM}}$ .

### 3.4 STATISTICAL MODELING

In this section, the statistical modeling of  $\beta$  for the square  $M$ -QAM and  $M$ -PAM constellations when  $M \in \{4, 16, 64\}$  is discussed. Also, several values of block length  $N$  are taken

---

<sup>2</sup> The Lognormal distribution is used since the statistical modeling in Section 3.4 shows that it is the best distribution to model  $\beta$  for  $M$ -PAM constellations.

into account and, for each one of them, the Monte Carlo method is applied with 100.000 iterations, which provides enough data for carrying out the statistical modeling for each block length, since  $\beta$  is an r.v. with an unknown statistical distribution. For the considered constellations, a comparative analysis is made considering a set of several statistical distributions ( $\mathcal{A} = \{\text{Birnbbaum-Saunders, Burr, Gamma, Gaussian, Logistic, Lognormal, Nakagami, Rayleigh, Rician, Weibull}\}$ ), which are empirically chosen based on the data set obtained for  $\beta$ . Also, circularly-symmetric Gaussian and Gaussian white random processes are respectively applied for  $M$ -QAM and  $M$ -PAM constellations.

The results are shown based on three chosen criteria in order to define the best statistical distribution that models  $\beta$ . They are the Maximum Likelihood Estimation (MLE), Akaike information criterion (AIC), and Bayesian information criterion (BIC) [63,64]. The best model is the one with maximum MLE and minimum AIC and BIC, which is selected based on the majority vote rule [65], agreeing with the methodology presented in [51].

Also, based on [51], with the purpose of facilitating the analysis of the MLE criterion, the parameter  $\rho_{A_i}[N]$  is used, which is defined as

$$\rho_{A_i}[N] \triangleq \left| 1 - \frac{\max_{\mathcal{A}} \text{MLE}[N]}{\text{MLE}[A_i, N]} \right|, \quad (3.27)$$

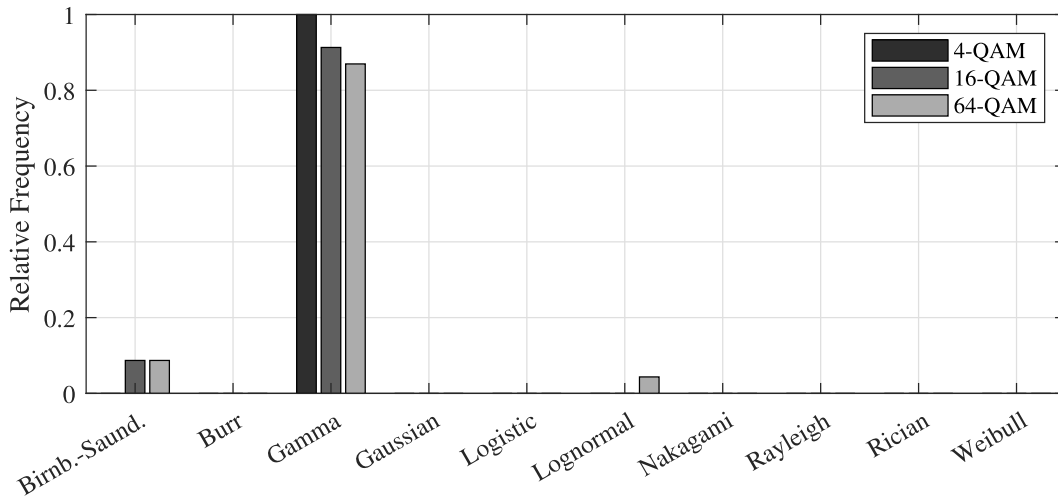
where  $\text{MLE}[A_i, N]$  is the value of the log-likelihood associated with one of the chosen statistical distributions ( $A_i$ ) belonging to the set of statistical distributions ( $\mathcal{A}$ ) when an  $N$ -length block is considered and  $\max_{\mathcal{A}} \text{MLE}[N]$  denotes the value of the log-likelihood related to the statistical distribution with the best statistical model. The parameter presented in (3.27) is of most importance since a particular statistical distribution can be chosen as the best model of  $\beta$  depending on the value of  $N$  and  $\rho_{A_i}[N]$  can compare the quality of fit of the statistical distributions in a quantitative manner.

### 3.4.1 $M$ -QAM Constellations

The first constellations to be investigated are the 4-QAM, 16-QAM, and 64-QAM. The relative frequency in which the statistical distributions are chosen as the best model for  $\beta$  is shown in Figure 8. Note that, for the 4-QAM constellation, the Gamma distribution was the only statistical distribution chosen as the best model for  $\beta$  regardless of the block length. Similarly, for both 16-QAM and 64-QAM constellations, the Gamma distribution was for the most part the best model. However, the Birnbbaum-Saunders and Lognormal distributions were chosen as the best models for some values of  $N$ . Also, it is important to emphasize that, as  $M$  increases, the Gamma distribution becomes less predominant in the process of choosing the best statistical model, i.e., other distributions become more relevant as  $M$  increases.

Thus, due to the fluctuation regarding the best statistical model for  $\beta$  in the 16-QAM and 64-QAM constellations, Table 2 presents  $\rho_{A_i}[N]$  of the three best statistical distributions when

Figure 8 – Relative frequency associated with the set of statistical distributions that best model  $\beta$  considering  $M$ -QAM constellations



Source: Personal collection.

a distribution distinct from the Gamma distribution is chosen as the best model for  $\beta$ . Note that even when a different distribution from Gamma is selected as the best model for  $\beta$ , the values of  $\rho_{A_i}[N]$  related to the Gamma distribution are substantially low. This is an important outcome favoring the use of the Gamma distribution as the best statistical model for  $\beta$  when an  $M$ -QAM constellation is considered since, even when the Gamma distribution is not chosen as the best model, it is still relatively close to the best one.

Table 2 – Values of  $\rho_{A_i}[N]$  for the 16-QAM and 64-QAM constellations when a distribution other than the Gamma distribution is chosen as the best model for  $\beta$

	16-QAM		
	Birnbaum-Saund.	Gamma	Lognormal
$\rho_{A_i}[600]$	0	0.000015	0.000003
$\rho_{A_i}[1000]$	0	0.000008	0.000001
	64-QAM		
	Birnbaum-Saund.	Gamma	Lognormal
$\rho_{A_i}[400]$	0.000004	0.000001	0
$\rho_{A_i}[600]$	0	0.000012	0.000002
$\rho_{A_i}[1000]$	0	0.000004	0.000001

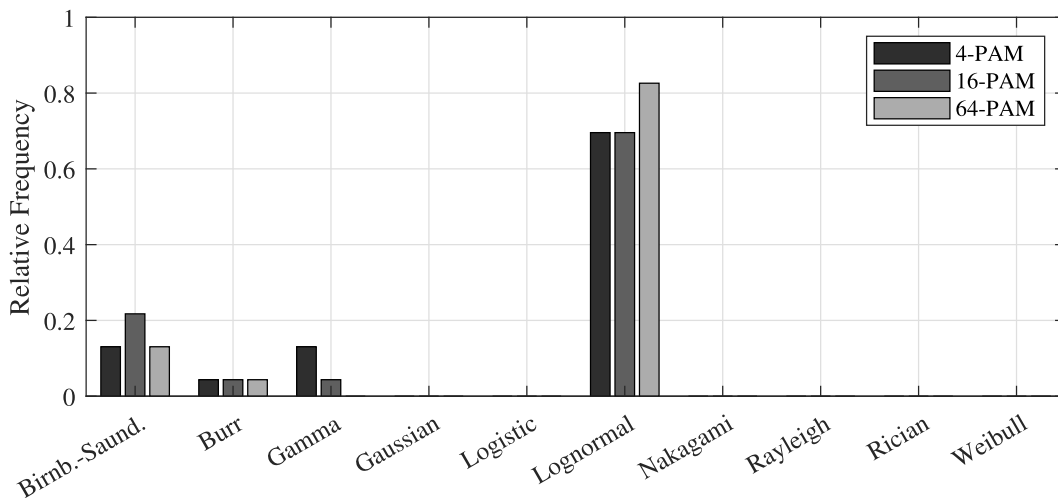
Source: Personal collection.

### 3.4.2 $M$ -PAM Constellations

Similar to the analysis presented for the  $M$ -QAM constellations, Figure 9 shows the relative frequency that the statistical distributions are chosen as the best model for  $\beta$  considering

the 4-PAM, 16-PAM, and 64-PAM constellations. Different from the  $M$ -QAM constellations, the Lognormal distribution was predominantly the best model for the  $M$ -PAM constellations. Also, for a few values of  $N$  the distributions Birnbaum-Saunders, Burr and Gamma were chosen as the best models. Moreover, on the contrary to what is experienced in the  $M$ -QAM constellations, for the  $M$ -PAM ones the predominant statistical distribution increases its chance of being the best statistical model for  $\beta$  as  $M$  increases.

Figure 9 – Relative frequency associated with the set of statistical distributions that best model  $\beta$  considering  $M$ -PAM constellations



Source: Personal collection.

Once again, due to the inconstancy regarding the best statistical model for the r.v.  $\beta$  in all three  $M$ -PAM constellations, Table 3 exhibits  $\rho_{A_i}[N]$  for the four best statistical distributions when a distribution distinct from the Lognormal distribution is chosen as the best model for  $\beta$ . Note that the Lognormal distribution performs significantly well when other distributions are chosen as the best model for  $\beta$ , which favors the use of such statistical distribution to model  $\beta$  in  $M$ -PAM constellations. Also, for the highlighted values of  $N$ , the Birnbaum-Saunders distribution is usually chosen as the best statistical model.

### 3.4.3 Similar Modeling Constellations

Due to the structure of some specific constellations, the modeling of the r.v.  $\beta$  can be generalized, which substantially simplifies the modeling process. Such simplification may arise when there is equality between  $\mathcal{E}_{x,\text{FBL}}$  and  $\mathcal{E}_x$ . For instance, the 4-QAM constellation presents a structure which is a type of amplitude constant constellation and, consequently,  $\mathcal{E}_{x,\text{FBL}} = \mathcal{E}_x$ . As a matter of fact, this is an important aspect of the r.v.  $\beta$  since the modeling of the 4-QAM constellation can be directly applied, for example, to a phase-shift keying (PSK) constellation with  $M = 4$ .

Table 3 – Values of  $\rho_{A_i}[N]$  for the 4-PAM, 16-PAM, and 64-PAM constellations when a distribution other than the Lognormal distribution is chosen as the best model for  $\beta$

4-PAM				
	Birnbaum-Saund.	Burr	Gamma	Lognormal
$\rho_{A_i}[10]$	0.010191	0	0.011035	0.001479
$\rho_{A_i}[100]$	0.000076	0.020103	0	0.000013
$\rho_{A_i}[300]$	0	0.009677	0.000061	0.000005
$\rho_{A_i}[400]$	0.000056	0.007654	0	0.000051
$\rho_{A_i}[450]$	0.000044	0.007760	0	0.000043
$\rho_{A_i}[700]$	0	0.006501	0.000085	0.000001
$\rho_{A_i}[1000]$	0	0.006072	0.000035	0.000001
16-PAM				
	Birnbaum-Saund.	Burr	Gamma	Lognormal
$\rho_{A_i}[10]$	0.010756	0	0.015700	0.001258
$\rho_{A_i}[300]$	0	0.009830	0.000246	0.000001
$\rho_{A_i}[450]$	0	0.008234	0.000223	0.000001
$\rho_{A_i}[500]$	0	0.008066	0.000284	0.000002
$\rho_{A_i}[600]$	0	0.007451	0.000292	0.000001
$\rho_{A_i}[900]$	0.000005	0.006271	0	0.000006
$\rho_{A_i}[1000]$	0	0.006237	0.000122	0.000001
64-PAM				
	Birnbaum-Saund.	Burr	Gamma	Lognormal
$\rho_{A_i}[10]$	0.009449	0	0.014665	0.000433
$\rho_{A_i}[200]$	0	0.012757	0.000846	0.000001
$\rho_{A_i}[600]$	0	0.007282	0.000094	0.000001
$\rho_{A_i}[1000]$	0	0.006164	0.000056	0.000001

Source: Personal collection.

### 3.5 MODELING OF PARAMETERS OF THE CHOSEN DISTRIBUTIONS

Based on the discussion presented in Section 3.4, it becomes clear which statistical distributions are the best models for  $\beta$  for the considered  $M$ -ary constellations. Therefore, the present section aims to define the parameters of each statistical distribution in order to fit into the model for the  $M$ -QAM and  $M$ -PAM constellations.

#### 3.5.1 $M$ -QAM Constellations

Given the analysis of the set of statistical distributions, it is evident that the Gamma distribution is the statistical distribution capable of better modeling the r.v.  $\beta$  considering the

$M$ -QAM constellations. With that in mind, the PDF of the Gamma distribution can be expressed as

$$f_{\beta}(x | k, \theta) = \frac{1}{\theta^k \Gamma(k)} x^{k-1} e^{-\frac{x}{\theta}}, \quad (3.28)$$

in which  $k$  and  $\theta$  denote, respectively, the shape and scale parameters of the Gamma distribution and  $\Gamma(\cdot)$  is the Gamma function. The MLE criterion and confidence intervals of 95% are used to estimate the parameters. Therefore, based on the estimations and the observation of the behavior of each parameter when  $N$  varies, the empirically defined functions used to model the set of parameters are defined as follows:

- First,  $k$  is modeled as a linear function of  $N$  and its mathematical equation can be given by

$$k[N] = \alpha_{k_1} N + \alpha_{k_2}, \quad (3.29)$$

where  $\alpha_{k_1}$  and  $\alpha_{k_2}$  are the coefficients of the linear function.

- The parameter  $\theta$  is modeled as a reciprocal function of  $N$  and its mathematical equation can be expressed as

$$\theta[N] = \frac{1}{\alpha_{\theta_1} N + \alpha_{\theta_2}}, \quad (3.30)$$

where  $\alpha_{\theta_1}$  and  $\alpha_{\theta_2}$  are the coefficients of the chosen function.

Therefore, Table 4 and Table 5 exhibit the values of each parameter coefficient for the three considered  $M$ -QAM constellations. Also, Table 6 and Table 7 show the values of each parameter obtained with its modeling function and the estimates with the confidence interval of 95% for 4-QAM, 16-QAM, and 64-QAM constellations. Note that for both parameters, the samples modeled by the modeling functions displayed in (3.29) and (3.30) are contained within the confidence interval of 95% for all three  $M$ -QAM constellations. Such outcome shows that both parameters present a similar behavior when compared to the defined modeling functions, regardless of the constellation order. Also, the chosen modeling functions proved to be quite adequate to model the set of parameters of a Gamma distribution when the  $M$ -QAM constellations are used in the adopted data communication system.



Table 4 – Coefficients of the modeling function for the parameter  $k$  of the Gamma distribution

	$\alpha_{k_1}$	$\alpha_{k_2}$
4-QAM	0.4998	-0.4478
16-QAM	0.4311	-0.3781
64-QAM	0.4202	-0.4279

Source: Personal collection.

Table 5 – Coefficients of the modeling function for the parameter  $\theta$  of the Gamma distribution

	$\alpha_{\theta_1}$	$\alpha_{\theta_2}$
4-QAM	0.5002	-0.5093
16-QAM	0.4316	-0.5452
64-QAM	0.4208	-0.5399

Source: Personal collection.

Table 6 – Values of  $k[N]$  achieved with its modeling function in comparison with the confidence interval of 95% for 4-QAM, 16-QAM, and 64-QAM constellations

	4-QAM				
	$N = 10$	$N = 50$	$N = 100$	$N = 500$	$N = 1000$
$k[N]$	4.5502	24.5422	49.5322	249.4522	499.3522
$k_{\min}$	4.4524	24.2518	49.0397	245.9833	492.9037
$k_{\max}$	4.5525	24.8132	50.1787	251.7124	504.3877
	16-QAM				
	$N = 10$	$N = 50$	$N = 100$	$N = 500$	$N = 1000$
$k[N]$	3.9329	21.1769	42.7319	215.1719	430.7219
$k_{\min}$	3.8677	20.9177	42.4347	212.2472	425.1431
$k_{\max}$	3.9543	21.4014	43.4198	217.1900	435.0478
	64-QAM				
	$N = 10$	$N = 50$	$N = 100$	$N = 500$	$N = 1000$
$k[N]$	3.7741	20.5821	41.5921	209.6721	419.7721
$k_{\min}$	3.7840	20.4505	41.2127	206.5943	414.7664
$k_{\max}$	3.8686	20.9233	42.1694	211.4054	424.4292

Source: Personal collection.

### 3.5.2 $M$ -PAM Constellations

Taking into account the discussion regarding the  $M$ -PAM constellations and the best statistical model considering a set of statistical distributions, the Lognormal distribution presented

Table 7 – Values of  $\theta[N]$  achieved with its modeling function in comparison with the confidence interval of 95% for 4-QAM, 16-QAM, and 64-QAM constellations

4-QAM					
	$N = 10$	$N = 50$	$N = 100$	$N = 500$	$N = 1000$
$\theta[N]$	0.22258	0.04082	0.02020	0.00401	0.00200
$\theta_{\min}$	0.22002	0.04029	0.01992	0.00397	0.00198
$\theta_{\max}$	0.22525	0.04123	0.02039	0.00407	0.00203
16-QAM					
	$N = 10$	$N = 50$	$N = 100$	$N = 500$	$N = 1000$
$\theta[N]$	0.26520	0.04754	0.02347	0.00465	0.00232
$\theta_{\min}$	0.26210	0.04701	0.02310	0.00461	0.00230
$\theta_{\max}$	0.26837	0.04812	0.02364	0.00471	0.00235
64-QAM					
	$N = 10$	$N = 50$	$N = 100$	$N = 500$	$N = 1000$
$\theta[N]$	0.27262	0.04878	0.02407	0.00477	0.00238
$\theta_{\min}$	0.26952	0.04818	0.02380	0.00473	0.00236
$\theta_{\max}$	0.27596	0.04930	0.02436	0.00484	0.00241

Source: Personal collection.

the best results. The PDF of the Lognormal distribution of an r.v.  $\beta$  is given by

$$f_{\beta}(x | \mu, \sigma) = \frac{1}{x\sigma\sqrt{2\pi}} e^{-\frac{(\ln x - \mu)^2}{2\sigma^2}}, \quad (3.31)$$

in which  $\mu$  and  $\sigma$  denote, respectively, the mean and the standard deviation of the Lognormal distribution. Again, the MLE criterion and confidence intervals of 95% are used to estimate the parameters. Therefore, based on the estimations and the observation of the behavior of each parameter when  $N$  varies, the set of parameters of the Lognormal distribution are modeled using the empirically defined functions as follows:

- The parameter  $\mu$  is modeled as a negative reciprocal function of  $N$ , which is given by

$$\mu[N] = -\frac{1}{\alpha_{\mu_1}N + \alpha_{\mu_2}}, \quad (3.32)$$

where  $\alpha_{\mu_1}$  and  $\alpha_{\mu_2}$  are the coefficients of the function.

- The parameter  $\sigma$ , as a function of  $N$ , is modeled with

$$\sigma[N] = \frac{1}{\alpha_{\sigma_1}\sqrt{N} + \alpha_{\sigma_2}}, \quad (3.33)$$

where  $\alpha_{\sigma_1}$  and  $\alpha_{\sigma_2}$  are the coefficients of the chosen function.

Thus, Table 8 and Table 9 show the values of each parameter coefficient for the three considered  $M$ -PAM constellations. Furthermore, Table 10 and Table 11 show the values of each parameter obtained with its modeling function and the estimates with the confidence interval of 95% for 4-PAM, 16-PAM, and 64-PAM constellations. It is notable that for the parameter  $\mu$  the confidence intervals of 95% cover all the samples obtained with the chosen modeling functions given by (3.32). Observe that, for the parameter  $\sigma$ , some samples obtained with the modeling function (3.33) are marginally out of the confidence intervals of 95%, mainly for  $N \geq 500$ . Also, the results yielded for both parameters show that the differences between the  $M$ -PAM constellations when the Lognormal distribution is chosen are nearly negligible. Finally, it is important to emphasize that the modeling functions chosen to model the parameters of the Lognormal distribution are suitable for the considered  $M$ -PAM constellations.

Table 8 – Coefficients of the modeling function for the parameter  $\mu$  of the Lognormal distribution

	$\alpha_{\mu_1}$	$\alpha_{\mu_2}$
4-PAM	1.4620	-1.6450
16-PAM	1.6280	-1.8690
64-PAM	1.6540	-2.0400

Source: Personal collection.

Table 9 – Coefficients of the modeling function for the parameter  $\sigma$  of the Lognormal distribution

	$\alpha_{\sigma_1}$	$\alpha_{\sigma_2}$
4-PAM	0.6359	-0.2454
16-PAM	0.6178	-0.2322
64-PAM	0.6172	-0.2339

Source: Personal collection.

### 3.6 NUMERICAL ANALYSES

In this section, three distinct case scenarios in which the FBL analysis can be applied are discussed. Case Studies I and II consider the digital communication system detailed in Section 3.1, in which transmitter and receiver are performing data communication without transmission energy knowledge. The former assumes that the CIR is known by both transmitter and receiver, while the latter considers that the CIR is unknown by the receiver. Case Study III is based on a typical theoretical view of PLS [66–70] as shown in Figure 10. In this scenario, it is

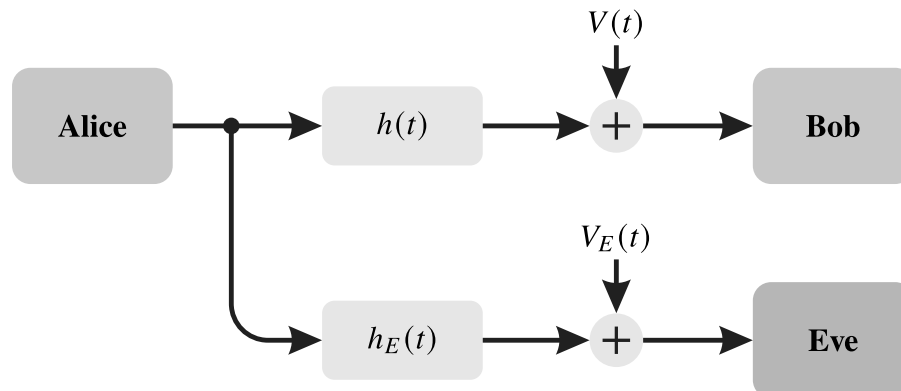
Table 10 – Values of  $\mu[N]$  achieved with its modeling function in comparison with the confidence interval of 95% for 4-PAM, 16-PAM, and 64-PAM constellations

4-PAM					
	$N = 10$	$N = 50$	$N = 100$	$N = 500$	$N = 1000$
$\mu[N]$	-0.07707	-0.01399	-0.00692	-0.00137	-0.00068
$\mu_{\min}$	-0.08075	-0.01544	-0.00776	-0.00190	-0.00094
$\mu_{\max}$	-0.07370	-0.01253	-0.00572	-0.00100	-0.00030
16-PAM					
	$N = 10$	$N = 50$	$N = 100$	$N = 500$	$N = 1000$
$\mu[N]$	-0.06939	-0.01257	-0.00621	-0.00123	-0.00061
$\mu_{\min}$	-0.07314	-0.01428	-0.00746	-0.00189	-0.00071
$\mu_{\max}$	-0.06591	-0.01130	-0.00537	-0.00097	-0.00006
64-PAM					
	$N = 10$	$N = 50$	$N = 100$	$N = 500$	$N = 1000$
$\mu[N]$	-0.06897	-0.01240	-0.00612	-0.00121	-0.00061
$\mu_{\min}$	-0.07284	-0.01463	-0.00731	-0.00158	-0.00080
$\mu_{\max}$	-0.06559	-0.01164	-0.00522	-0.00065	-0.00014

Source: Personal collection.

considered the presence of an eavesdropper (Eve) in the system, which is capable of overhearing the signal transmitted from the transmitter (Alice) to the receiver (Bob). Note that Alice, Bob, and Eve make use of the transmitter and receiver devices detailed in Section 3.1. Case Study I is discussed in Subsection 3.6.1 while the other ones are detailed in Subsection 3.6.2. Case Studies II and III are united since the same formulation can be applied for both of them as justified in Subsection 3.6.2. The discussed results consider  $N \in \{10, 50, 100, 500, 1000\}$  and the noise variances of Bob ( $\sigma_v^2$ ) and Eve ( $\sigma_{v_E}^2$ ) are defined so that  $\sigma_v^2 = \sigma_{v_E}^2 = 10^{-6}$ .

Figure 10 – Block diagram of a wiretap channel model



Source: Block diagram based on [69].

Table 11 – Values of  $\sigma[N]$  achieved with its modeling function in comparison with the confidence interval of 95% for 4-PAM, 16-PAM, and 64-PAM constellations

4-PAM					
	$N = 10$	$N = 50$	$N = 100$	$N = 500$	$N = 1000$
$\sigma[N]$	0.56641	0.23523	0.16357	0.07156	0.05034
$\sigma_{\min}$	0.56650	0.23329	0.16350	0.07254	0.05125
$\sigma_{\max}$	0.57149	0.23535	0.16494	0.07318	0.05170
16-PAM					
	$N = 10$	$N = 50$	$N = 100$	$N = 500$	$N = 1000$
$\sigma[N]$	0.58090	0.24176	0.16819	0.07363	0.05180
$\sigma_{\min}$	0.58063	0.23905	0.16782	0.07439	0.05270
$\sigma_{\max}$	0.58574	0.24116	0.16930	0.07505	0.05316
64-PAM					
	$N = 10$	$N = 50$	$N = 100$	$N = 500$	$N = 1000$
$\sigma[N]$	0.58212	0.24211	0.16840	0.07371	0.05186
$\sigma_{\min}$	0.58226	0.24034	0.16814	0.07489	0.05269
$\sigma_{\max}$	0.58739	0.24246	0.16962	0.07555	0.05315

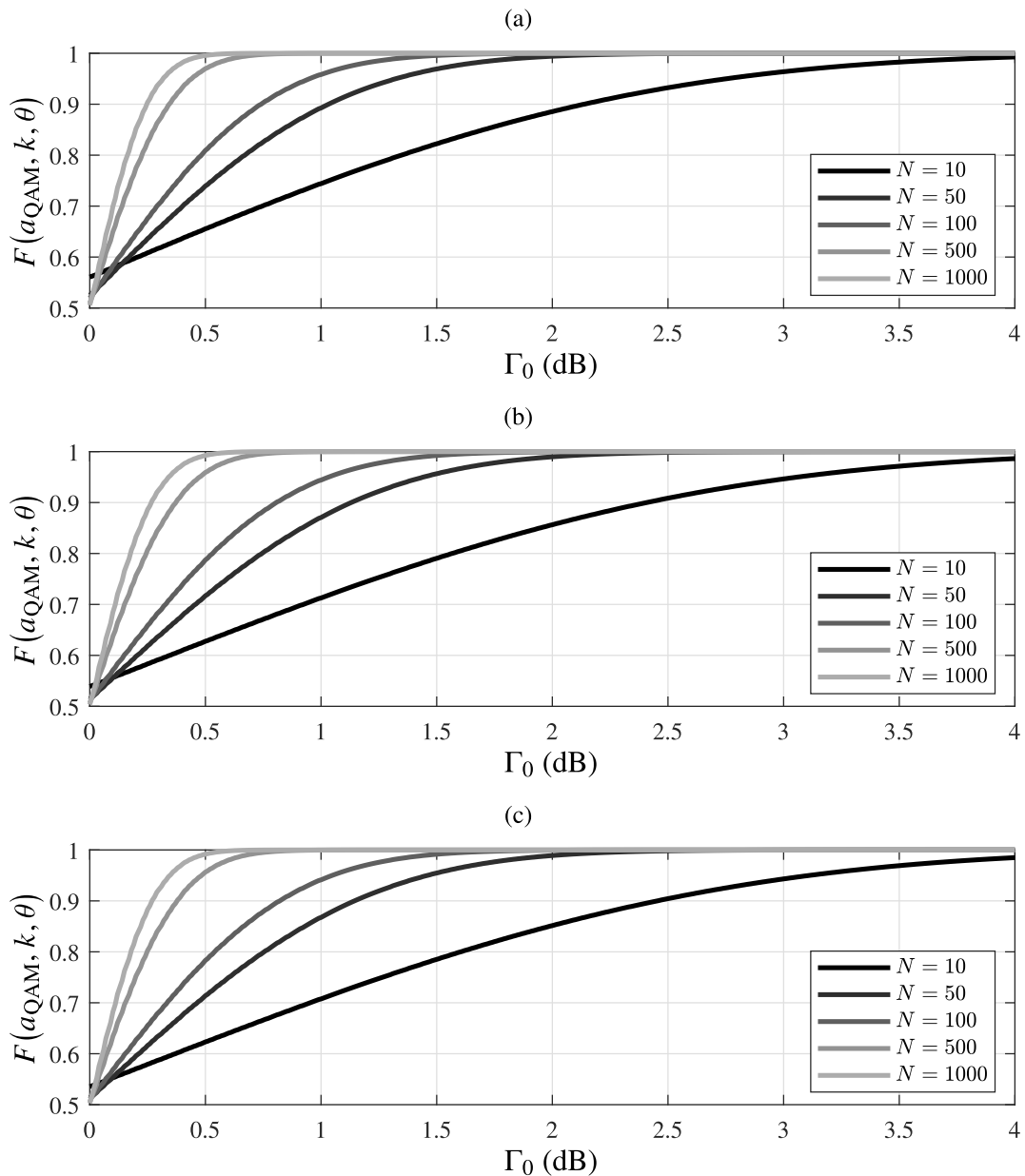
Source: Personal collection.

### 3.6.1 Case Study I

In this case, it is assumed that  $|h|^2 = 1$  (0 dB) and that it is completely known by the receiver. With that in mind, Figure 11 and Figure 12 display the probabilities of ensuring the SEP upper bounds when distinct values of  $\Gamma_0$  are used for  $M$ -QAM and  $M$ -PAM constellations, respectively, and the receiver is unaware of the transmission energy. It is clear that as  $\Gamma_0$  or  $N$  increases, the probabilities of ensuring the SEP upper bounds also increase. However, the higher the order of the constellation  $M$ , the lower the probabilities. Regardless of the value of  $N$ , note that QAM offers better performance than pulse amplitude modulation (PAM) in the FBL regime, under the same channel conditions. Regarding the chosen sizes of  $M$ -QAM constellations, it is notable the remarkable difference between the 4-QAM constellation when compared to the other  $M$ -QAM constellations since 4-QAM is a type of amplitude constant constellation. For example, when  $\Gamma_0 = 1$  dB,  $F(a_{\text{QAM}}, k, \theta) = 0.74$  for the 4-QAM constellation, whereas for the other  $M$ -QAM constellations  $F(a_{\text{QAM}}, k, \theta) \approx 0.7$ . On the other hand, the performance associated with the sizes of  $M$ -PAM constellations shows small differences when the constellation size changes. Since the discussion in Case Study I regards the data communication only between transmitter and receiver, based on Figure 11 and Figure 12, intuitively it would be advantageous for the system to be designed with high values of  $\Gamma_0$ . However, despite such assumption being accurate based on the presented results, the increase in  $\Gamma_0$  causes an escalation of the required

power to transmit signals that satisfy the designed SEP conditions of the system. Therefore, the data communication system needs to be designed taking into account several features and considering a trade-off between the probability of ensuring the SEP upper bounds and the required  $\Gamma_0$  when the FBL regime is considered.

Figure 11 – Values of  $F(a_{\text{QAM}}, k, \theta)$  when the receiver is aware of  $h$  for (a) 4-QAM, (b) 16-QAM, and (c) 64-QAM constellations

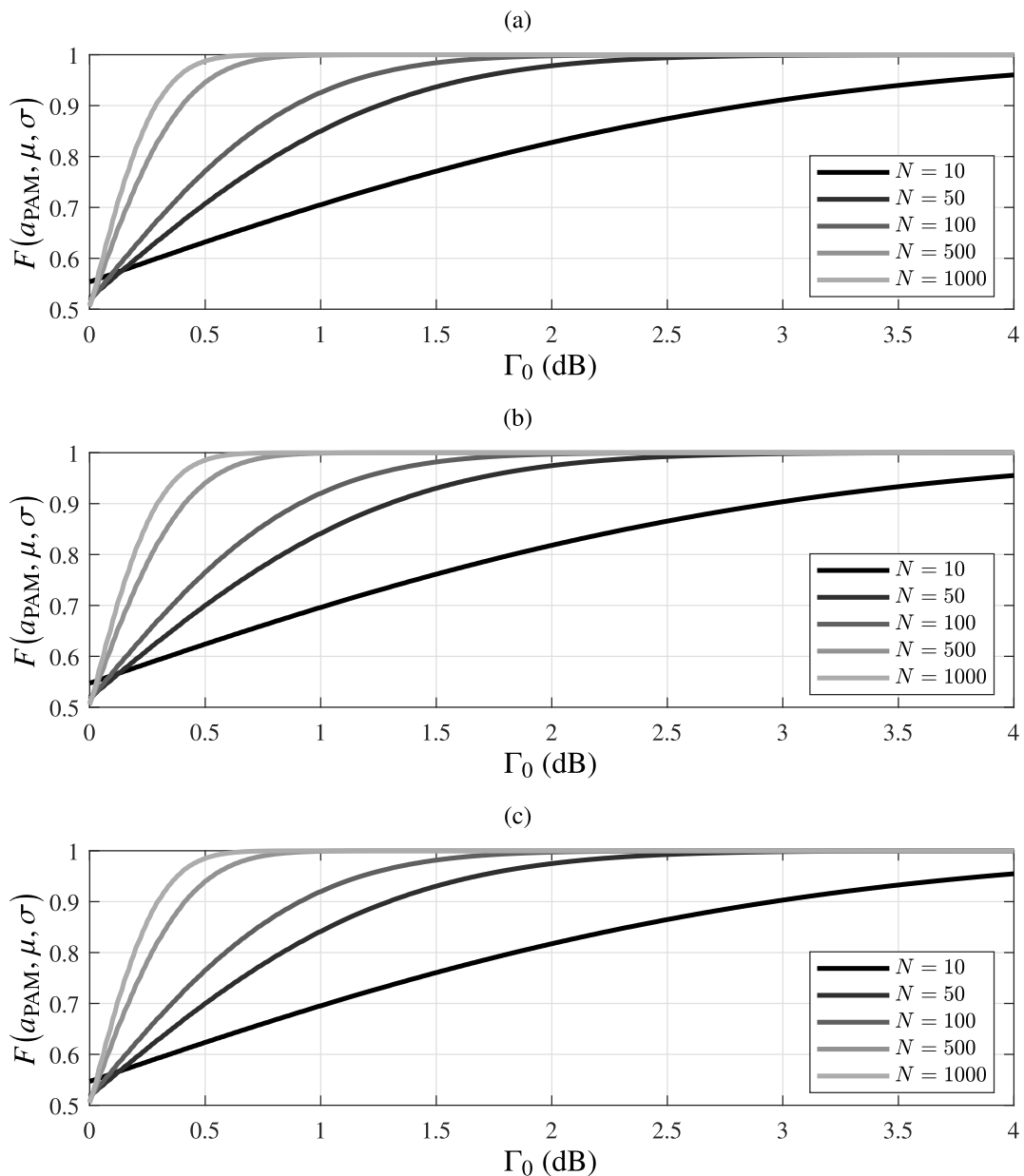


Source: Personal collection.

### 3.6.2 Case Studies II and III

Initially, Case Study II is analyzed, in which the receiver in the digital communication system detailed in Section 3.1 does not know the value of  $|h|^2$ . In this scenario, the lack of

Figure 12 – Values of  $F(a_{\text{PAM}}, \mu, \sigma)$  when the receiver is aware of  $h$  for (a) 4-PAM, (b) 16-PAM, and (c) 64-PAM constellations



Source: Personal collection.

this information results in a loss in the probability of ensuring the SEP upper bound. In this regard, Figure 13 and Figure 14 show the probabilities of ensuring the SEP upper bounds for the  $M$ -QAM and  $M$ -PAM constellations, respectively, when the data communication between the transmitter and receiver is designed with  $\Gamma_0 = 1$  dB. Also, it is assumed that the receiver considers  $|h|^2 = 1$  (0 dB) but it is not the real value of  $|h|^2$ . Consequently, it allows us to quantify the losses when there is a difference between the real value of  $|h|^2$  and the one that is supposed to be known by the receiver (i.e.,  $\Delta|h|^2 = 1 - |h|^2$ ). Note that if there is a 3 dB increase in the value of  $|h|^2$  (i.e.,  $\Delta|h|^2(\text{dB}) = 3$ ), then reasonably high values of  $F(a_{\text{QAM}}, k, \theta)$

and  $F(a_{\text{PAM}}, \mu, \sigma)$  when  $N \gg 10$  are attained. On the other hand, if the real value of  $|h|^2$  is 3 dB below the value that is supposed to be known by the receiver (i.e.,  $\Delta|h|^2(\text{dB}) = -3$ ), then reasonably low values of  $F(a_{\text{QAM}}, k, \theta)$  and  $F(a_{\text{PAM}}, \mu, \sigma)$  are attained for every considered  $N$ . As a consequence, regarding the system designed with  $\Gamma_0 = 1$  dB (see Figs. 13-14), the receiver can only ensure high reliable data communication when  $\Delta|h|^2(\text{dB}) \geq -0.5$  and  $N$  is large (e.g.,  $N \geq 500$ ). Also, if  $N$  is considerably small (e.g.,  $N \approx 10$ ), then the impact of the knowledge of the CIR is less pronounced. Moreover, small values of  $N$  seems to be useful when  $\Delta|h|^2(\text{dB}) \leq 0$  since  $F(a_{\text{QAM}}, k, \theta)$  and  $F(a_{\text{PAM}}, \mu, \sigma)$  present smoother variations in comparison to large values of  $N$ . In other words, the use of digital communication systems in situations where the value of  $|h|^2$  is below a hypothetical value known by the receiver is less unreliable.

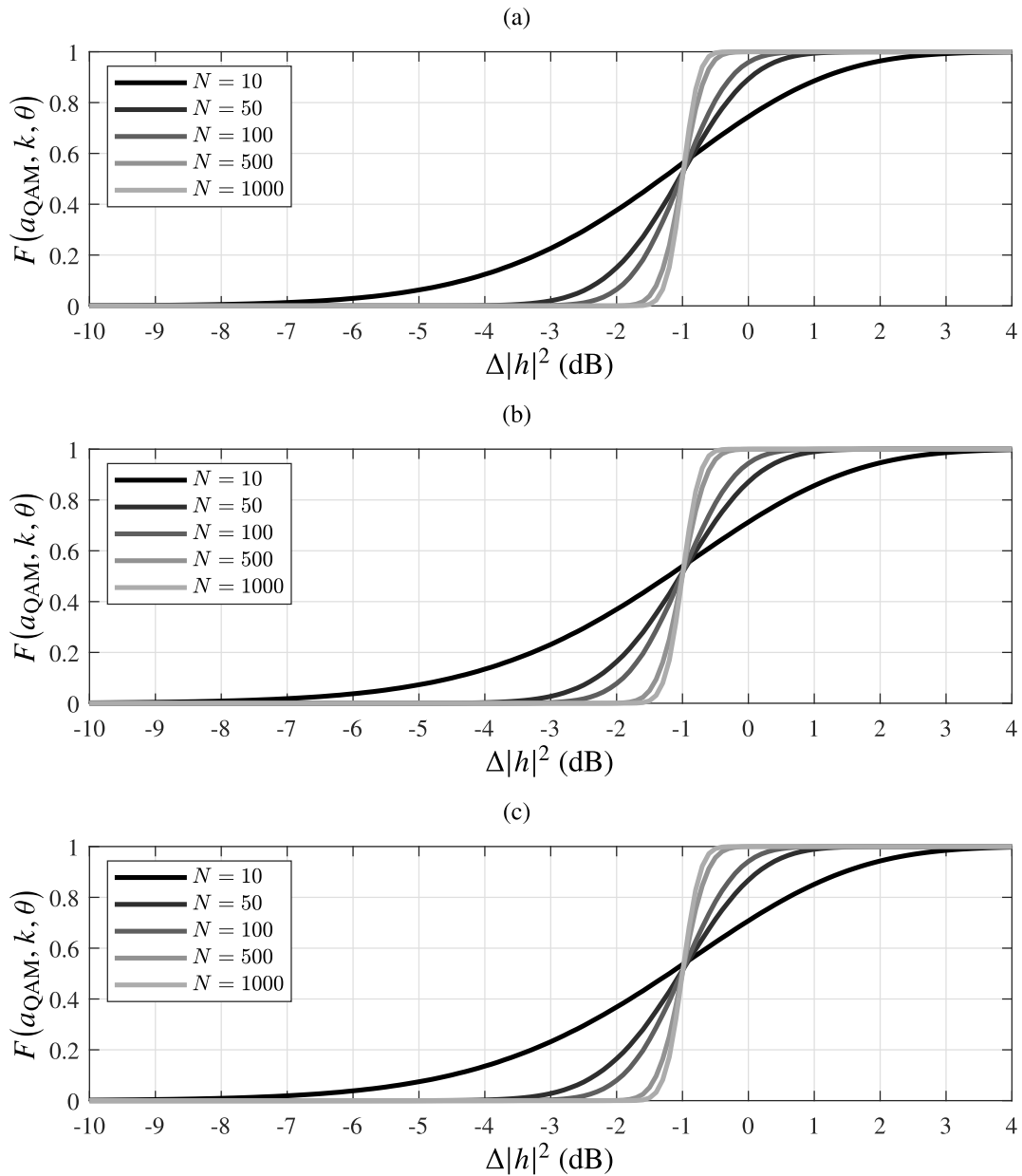
It is important to highlight that Figure 13 and Figure 14 are also valid for Case Study III, in which the data communication system is shown by Figure 10. Keep in mind that in this case, the data communication between Alice and Bob under the presence of Eve is considered. With the purpose of carrying out our analysis, it is assumed that Bob knows  $|h|^2$  and, as a consequence, the results presented in Subsection 3.6.1 apply to Bob. On the other hand, Eve has no knowledge of  $|h_E|^2$  and, consequently, the results showed in Figure 13 and Figure 14 can be directly applied to Eve with the replacement of  $h$  by  $h_E$ . In this new scenario, the interpretation of the probabilities of ensuring the SEP upper bounds by a malicious device, which is capable of eavesdropping data at the physical layer level, shows that the relative distance among Alice, Bob, and Eve define the attenuation level of the channel, and it is an important issue to be considered. For instance, it would be beneficial for the presented scenario of data communication between Alice and Bob, which considers  $\Gamma_0 = 1$  dB, to operate under the condition that  $\Delta|h_E|^2 < -3$  dB for the values of  $N > 10$  since it ensures that Eve will not be able to perform a successful attack. Also, if  $N$  is small (e.g.,  $N = 10$ ) and  $\Delta|h_E|^2 \geq -3$  dB, then an eavesdropper can overhear part of the transmitted information, as shown by the values of  $F(a_{\text{QAM}}, k, \theta)$  and  $F(a_{\text{PAM}}, \mu, \sigma)$  when  $N = 10$ . Consequently, the results show that the use of reduced block lengths in data communication systems may offer opportunities for an eavesdropper to perform successful attacks. Furthermore, if  $\Delta|h_E|^2 \geq 0$  dB, then Eve becomes a serious threat particularly when  $N$  is large.

### 3.7 SUMMARY

This chapter has discussed the SEP of an uncoded and single-carrier digital communication system when short and finite-length blocks of symbols are transmitted, and neither the transmission energy nor the channel state information are known by the receiver. The randomness yielded by the lack of such information was modeled as a single random variable, which is associated with estimates of the noise variance and the constellation energies obtained by the receiver. To circumvent this issue, the use of the so-called extra gap factor to undermine the



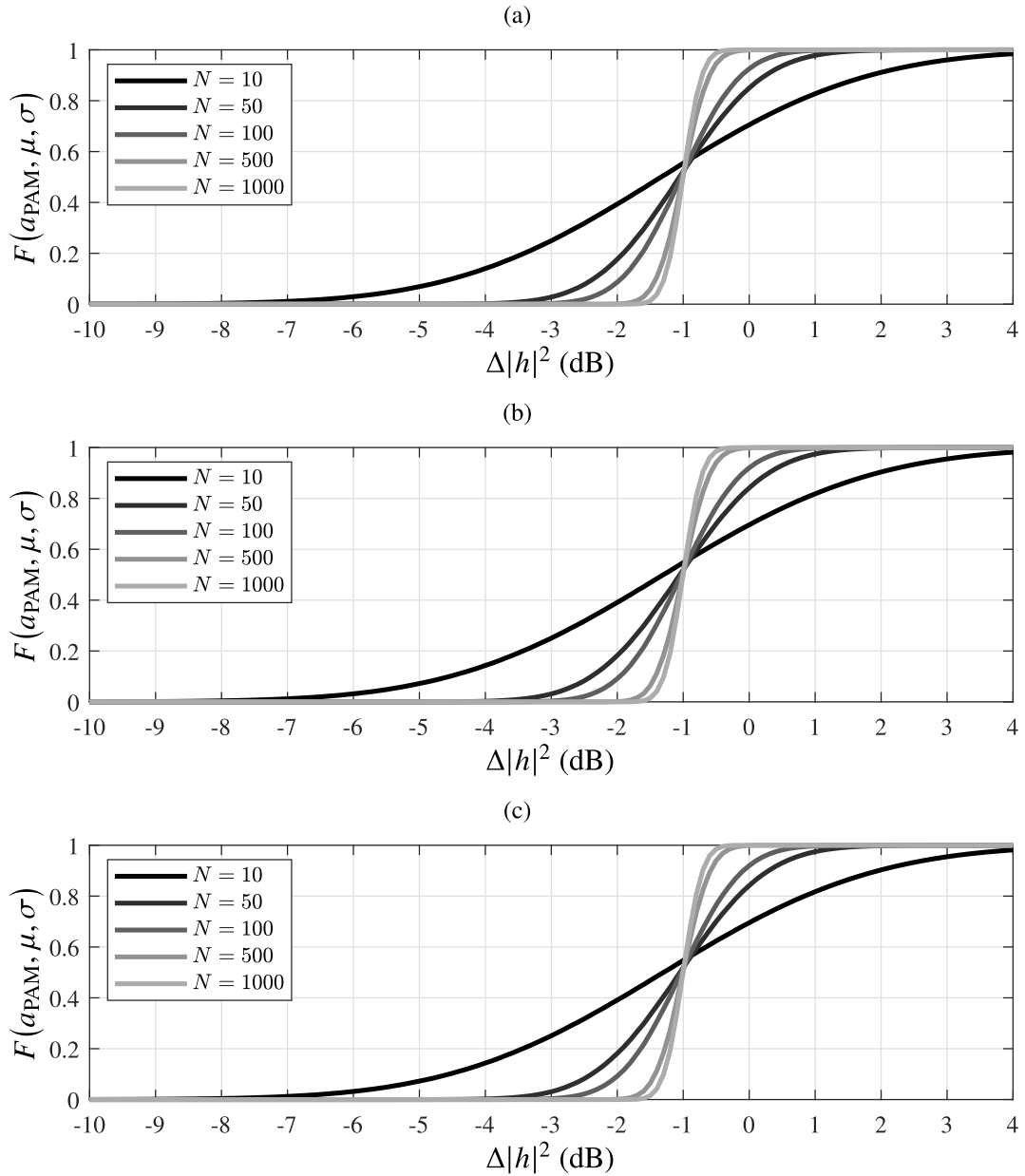
Figure 13 – Values of  $F(a_{\text{QAM}}, k, \theta)$  when the receiver is unaware of  $h$  and  $\Gamma_0 = 1$  dB for (a) 4-QAM, (b) 16-QAM, and (c) 64-QAM constellations



Source: Personal collection.

impact of such randomness was proposed. Also, to statistically evaluate the consequences of the lack of these pieces of information, models of this random variable were presented for  $M$ -QAM and  $M$ -PAM constellations. Finally, numerical analyses showed that, when the receiver knows the CSI, reasonable values of the extra gap factor are necessary to ensure reliable data communication. On the other hand, when the CSI is unknown by the receiver, longer block lengths or high value of the extra gap factor are crucial for ensuring reliability in the data communication system, especially in the presence of a malicious eavesdrop device, which is capable of overhearing the signal transmitted between Alice and Bob.

Figure 14 – Values of  $F(a_{\text{PAM}}, \mu, \sigma)$  when the receiver is unaware of  $h$  and  $\Gamma_0 = 1$  dB for (a) 4-PAM, (b) 16-PAM, and (c) 64-PAM constellations



Source: Personal collection.

## 4 CONCLUSION

This thesis has discussed the resource allocation for PLC systems based on the HS-OFDM scheme, specifically two enhancements for the TCRA technique were proposed, and has introduced the discussion about the FBL regime in a single-carrier digital communication system, addressing the peculiarities of such a regime and the changes brought out with it. Both discussions were carried out with the focus on the analysis of SER in the resource allocation discussion and SEP in the FBL regime discussion.

In Chapter 2, partial ETCRA and ETCRA were introduced, which are enhanced versions of TCRA, for ensuring the non-violation of an SER upper bound to the TCRA technique. The enhanced version were achieved based on two main modifications to the original one. The first proposed enhancement – which considers the use of the worst  $n$ SNR of the set of microslots in the resource allocation problem – is of great importance, since failure to comply with an SER upper bound results in loss of effective data rate due to the necessity of constant retransmissions that may be required for achieving an acceptable performance of OFDM-based PLC systems. In addition, a new calculation was presented for the correlation between microslots within the same cycle of the mains signal. Such correlation is more representative for the conditions of the data communication medium since it considers all subcarriers on the evaluation instead of a parameter resulted of previous processing and, consequently, possessing less information of the data communication medium. Therefore, based on a set of measured data composed of in-home PLC channels estimates and additive noise measurements obtained from a measurement campaign, a comparative analysis between the TCRA, partial ETCRA and ETCRA techniques was carried out considering two parameters: data rate loss and computational complexity reduction. Similar to TCRA, numerical results showed that ETCRA offers a trade-off between data rate and computational complexity and yields data rates relatively lower than those obtained with TCRA, when both modifications are taken into account. Moreover, by considering the partial ETCRA, it was shown that the new way of evaluating correlation results in higher reductions of computational complexity. Finally, it was shown that both enhanced versions ensure a non-violation of an SER upper bound established by the gap from the Shannon capacity curve while TCRA violates the SER upper bound in several microslots. As a result, both enhanced versions improve the overall performance of the resource allocation process in PLC systems.

Chapter 3 has addressed the probabilities of ensuring a target SEP, which is designed for the system based on the required SNR at the receiver, associated with the FBL regime in a single-carrier digital communication system when the receiver has knowledge or not of the CSI. Considering the lack of information of transmission power, it was shown, in the FBL regime, that the required SNR and, consequently, the target SEP can no longer be accurately achieved. Such circumstances take place as a result of the randomness introduced into the data communication system by both the noise variance and the signal energy. Therefore, in order

to circumvent the issue of ensuring the target SEP in the FBL regime, the addition of an extra gap factor was proposed, which evaluation is achieved based on the statistical modeling of the r.v. capable of modeling the randomness of the FBL regime. Thus, a comparative analysis was presented, based on a set of statistical distributions, of which statistical distribution best models the r.v. for  $M$ -QAM and  $M$ -PAM constellations, respectively. In the sequel, it was shown that the best statistical distributions for each one of the considered constellations are the Gamma distribution for  $M$ -QAM and the Lognormal distribution for  $M$ -PAM. Also, the parameters of each statistical distribution were modeled, based on empirically defined functions, in terms of the block length and validated comparing with an estimation with a confidence interval of 95%. Finally, three distinct case scenarios were discussed: Case Studies I and II regarded data communication among transmitter and receiver, where the former considered the awareness of the CSI by the receiver while the latter considered that the receiver was unaware of such information. Case Study III contemplated a typical PLS scenario in which a malicious device (Eve) eavesdrops upon the data exchanged between Alice and Bob. The results regarding the probabilities of ensuring SEP upper bounds when using  $M$ -QAM and  $M$ -PAM constellations were investigated and the usefulness of an extra gap factor to improve performance in a point-to-point data communication with and without the presence of an eavesdropping device under the FBL regime was discussed. For Case Study I, the performance obtained with QAM was better than the one achieved with PAM. Also, it was notable the discrepancy between the 4-QAM constellation and the other analyzed  $M$ -QAM constellations. Regarding Case Studies II and III, the impact on the lack of knowledge of the CIR was discussed, for both the receiving and the malicious devices, when the data communication system is designed with  $\Gamma_0 = 1$  dB. For both cases, smaller block lengths resulted in less variation on the probabilities of ensuring the SEP upper bounds. Such an outcome implies that the smaller the block length, the greater the restrictions that need to be imposed into the system to protect the data exchanged between communication devices against the presence of a malicious device.

#### 4.1 FUTURE WORKS

A list of future works is as follows:

- To formulate the statistical modeling for several types of constellations in order to determine the best statistical distribution and outline the results for future studies.
- To investigate the FBL regime for types of communication channel models different from the LTI channel, such as LPTV channels which allows the exploit of the time periodicity aspect of the communication channels and random channels.
- To analyze the FBL regime and the addition of an extra gap factor to a multi-carrier digital communication system with purpose of taking advantage of resource allocation techniques such as the ETCRA technique.

## REFERENCES

- [1] M. P. Tcheou, L. Lovisollo, M. V. Ribeiro, E. A. B. da Silva, M. A. M. Rodrigues, J. M. T. Romano, and P. S. R. Diniz, "The compression of electric signal waveforms for smart grids: State of the art and future trends," *IEEE Transactions on Smart Grid*, vol. 5, no. 1, pp. 291–302, Jan. 2014.
- [2] L. d. M. B. A. Dib, V. Fernandes, M. de L. Filomeno, and M. V. Ribeiro, "Hybrid PLC/wireless communication for smart grids and internet of things applications," *IEEE Internet of Things Journal*, vol. 5, no. 2, pp. 655–667, Apr. 2018.
- [3] C. R. Miranda, F. P. V. de Campos, and M. V. Ribeiro, "The prototype implementation of an IoT-based framework for energy reliability and asset security in base stations," in *XXXVII Simpósio Brasileiro de Telecomunicações e Processamento de Sinais*, Oct. 2019.
- [4] S. Fang, L. D. Xu, Y. Zhu, J. Ahati, H. Pei, J. Yan, and Z. Liu, "An integrated system for regional environmental monitoring and management based on internet of things," *IEEE Transactions on Industrial Informatics*, vol. 10, no. 2, pp. 1596–1605, May 2014.
- [5] G. R. Colen, L. G. de Oliveira, A. J. Han Vinck, and M. V. Ribeiro, "Resource allocation in OFDM-based PLC systems impaired by additive impulsive gaussian noise," in *International Symposium on Power Line Communications and its Applications*, Mar. 2016, pp. 70–75.
- [6] T. N. Vo, K. Amis, T. Chonavel, and P. Siohan, "Achievable throughput optimization in OFDM systems in the presence of interference and its application to power line networks," *IEEE Transactions on Communications*, vol. 62, no. 5, pp. 1704–1715, May 2014.
- [7] Z. Liu, X. Tao, and W. ur Rehman, "Resource allocation for two-way amplify and forward OFDM relay networks," *China Communications*, vol. 14, no. 8, pp. 76–82, Aug. 2017.
- [8] C. Kaiser, N. Mitschke, and K. Dostert, "Cyclic bit loading for adaptive OFDM in narrowband power line communications," in *IEEE International Symposium on Power Line Communications and its Applications*, Apr. 2018, pp. 1–6.
- [9] Y. Chen, X. Hu, and Z. Tan, "Power allocation for OFDM-DF cooperative communication," in *International Conference on Communications and Mobile Computing*, Apr. 2011, pp. 319–322.
- [10] L. G. de Oliveira, G. R. Colen, A. J. H. Vinck, and M. V. Ribeiro, "Resource allocation in HS-OFDM-based PLC systems: A tutorial," *Journal of Communication and Information Systems*, vol. 33, no. 1, Oct. 2018.
- [11] S. Morosi, D. Marabissi, Enrico Del Re, R. Fantacci, and N. Del Santo, "A rate adaptive bit-loading algorithm for in-building power-line communications based on DMT-modulated systems," *IEEE Transactions on Power Delivery*, vol. 21, no. 4, pp. 1892–1897, Oct. 2006.
- [12] Junhong Hui and Yongxing Zhou, "Enhanced rate adaptive resource allocation scheme in downlink OFDMA system," in *IEEE Vehicular Technology Conference*, vol. 5, May 2006, pp. 2464–2468.

- [13] F. Pancaldi, F. Gianaroli, and G. M. Vitetta, "Bit and power loading for narrowband indoor powerline communications," *IEEE Transactions on Communications*, vol. 64, no. 7, pp. 3052–3063, Jul. 2016.
- [14] X. Wu and Y. Rong, "Optimal power allocation for non-regenerative multicarrier relay-assisted PLC systems with QoS constraints," in *IEEE International Symposium on Power Line Communications and Its Applications*, Mar. 2015, pp. 142–147.
- [15] C. Wei, L. Qiu, and J. Zhu, "Margin adaptive optimization in multi-user MISO-OFDM systems under rate constraint," *Journal of Communications and Networks*, vol. 9, no. 2, pp. 112–117, Jun. 2007.
- [16] Z. Marijic, Z. Ilic, and A. Bazant, "Fixed-data-rate power minimization algorithm for OFDM-based power-line communication networks," *IEEE Transactions on Power Delivery*, vol. 25, no. 1, pp. 141–149, Jan. 2010.
- [17] A. M. Tonello, S. D'Alessandro, and L. Lampe, "Cyclic prefix design and allocation in bit-loaded OFDM over power line communication channels," *IEEE Transactions on Communications*, vol. 58, no. 11, pp. 3265–3276, Nov. 2010.
- [18] A. M. Tonello, S. D'Alessandro, and L. Lampe, "Bit, tone and cyclic prefix allocation in OFDM with application to in-home PLC," in *IFIP Wireless Days*, Nov. 2008, pp. 1–5.
- [19] Y. Zhou, J. Chen, and Y. Kuo, "Cooperative cross-layer resource allocation for self-healing in interworking of WLAN and femtocell systems," *IEEE Communications Letters*, vol. 21, no. 1, pp. 136–139, Jan. 2017.
- [20] C. Zhong and L. Yang, "Cross-layer scheduling and dynamic resource allocation for downlink multiuser MIMO systems with limited feedback," in *International Workshop on Cross Layer Design*, Sep. 2007, pp. 1–4.
- [21] R. Yang, C. Yuan, and K. Yang, "Cross layer resource allocation of delay sensitive service in OFDMA wireless systems," in *IEEE International Conference on Circuits and Systems for Communications*, May 2008, pp. 862–866.
- [22] Z. Xu, M. Zhai, and J. Lu, "Crosslayer optimization of user scheduling and resource allocation in power-line communication systems," *IEEE Transactions on Power Delivery*, vol. 26, no. 3, pp. 1449–1458, Jul. 2011.
- [23] A. M. Sarafi, A. E. Drougas, and P. G. Cottis, "Cross-layer resource allocation in medium-voltage broadband over power-line networks," *IEEE Transactions on Power Delivery*, vol. 27, no. 4, pp. 2247–2254, Oct. 2012.
- [24] M. A. Tunç, E. Perrins, and L. Lampe, "Optimal LPTV-aware bit loading in broadband PLC," *IEEE Transactions on Communications*, vol. 61, no. 12, pp. 5152–5162, 2013.
- [25] G. R. Colen, H. Schettino, D. Fernandes, L. M. Sirimarco, F. P. V. de Campos, W. A. Finamore, H. A. Latchman, and M. V. Ribeiro, "A temporal compressive resource allocation technique for complexity reduction in PLC transceivers," *Transactions on Emerging Telecommunications Technologies*, vol. 28, no. 2, p. e2951, 2017, e2951 ett.2951.
- [26] G. R. Colen, L. G. de Oliveira, A. J. H. Vinck, and M. V. Ribeiro, "A spectral compressive resource allocation technique for PLC systems," *IEEE Transactions on Communications*, vol. 65, no. 2, pp. 816–826, Feb. 2017.

- [27] L. Gaudio, T. Ninacs, T. Jerkovits, and G. Liva, “On the performance of short tail-biting convolutional codes for ultra-reliable communications,” in *International ITG Conference on Systems, Communications and Coding*, Feb. 2017, pp. 1–6.
- [28] K. Zhang, J. Jiao, Z. Huang, S. Wu, and Q. Zhang, “Finite block-length analog fountain codes for ultra-reliable low latency communications,” *IEEE Transactions on Communications*, vol. 68, no. 3, pp. 1391–1404, Mar. 2020.
- [29] H. Ko and S. Pack, “Neighbor-aware energy-efficient monitoring system for energy harvesting internet of things,” *IEEE Internet of Things Journal*, vol. 6, no. 3, pp. 5745–5752, Jun. 2019.
- [30] A. Mukherjee, “Physical-layer security in the internet of things: Sensing and communication confidentiality under resource constraints,” *Proceedings of the IEEE*, vol. 103, no. 10, pp. 1747–1761, Oct. 2015.
- [31] W. Li, H. Song, and F. Zeng, “Policy-based secure and trustworthy sensing for internet of things in smart cities,” *IEEE Internet of Things Journal*, vol. 5, no. 2, pp. 716–723, Apr. 2018.
- [32] T. Wang, M. Z. A. Bhuiyan, G. Wang, L. Qi, J. Wu, and T. Hayajneh, “Preserving balance between privacy and data integrity in edge-assisted internet of things,” *IEEE Internet of Things Journal*, vol. 7, no. 4, pp. 2679–2689, Apr. 2020.
- [33] T. M. Cover and J. A. Thomas, *Elements of Information Theory*. Wiley-Interscience, Jul. 2006.
- [34] Y. Polyanskiy, H. V. Poor, and S. Verdú, “Channel coding rate in the finite blocklength regime,” *IEEE Transactions on Information Theory*, vol. 56, no. 5, pp. 2307–2359, May 2010.
- [35] Y. Polyanskiy, H. V. Poor, and S. Verdú, “Dispersion of gaussian channels,” in *IEEE International Symposium on Information Theory*, Jun. 2009, pp. 2204–2208.
- [36] J. Park and D. Park, “A new power allocation method for parallel AWGN channels in the finite block length regime,” *IEEE Communications Letters*, vol. 16, no. 9, pp. 1392–1395, Sep. 2012.
- [37] Z. Mei, M. Johnston, S. Le Goff, and L. Chen, “Finite length analysis of low-density parity-check codes on impulsive noise channels,” *IEEE Access*, vol. 4, pp. 9635–9642, 2016.
- [38] M. D. Qureshi and W. H. Mow, “Improved performance bounds for finite-block-length network coded systems with polluted packet recycling,” *IEEE Wireless Communications Letters*, vol. 6, no. 1, pp. 6–9, Feb. 2017.
- [39] Y. Long, Y. Gao, and T. Yang, “Research on ultra-reliable and low-latency wireless communications in smart factory with finite block-length,” in *International Conference on Communications in China*, Aug. 2018, pp. 158–162.
- [40] J. Cao, X. Zhu, Y. Jiang, Y. Liu, and F. Zheng, “Joint block length and pilot length optimization for URLLC in the finite block length regime,” in *IEEE Global Communications Conference*, Dec. 2019, pp. 1–6.

- [41] S. Yan, B. He, Y. Cong, and X. Zhou, "Covert communication with finite blocklength in AWGN channels," in *IEEE International Conference on Communications*, May 2017, pp. 1–6.
- [42] N. Letzepis, "A finite block length achievability bound for low probability of detection communication," in *International Symposium on Information Theory and Its Applications*, Oct. 2018, pp. 752–756.
- [43] H. Tang, J. Wang, and Y. R. Zheng, "Covert communications with extremely low power under finite block length over slow fading," in *IEEE Conference on Computer Communications Workshops*, Apr. 2018, pp. 657–661.
- [44] M. Baldi, N. Maturo, G. Ricciutelli, and F. Chiaraluce, "Physical layer security over fading wiretap channels through classic coded transmissions with finite block length and discrete modulation," *Physical Communication*, vol. 37, p. 100829, Aug. 2019.
- [45] N. Papandreou and T. Antonakopoulos, "Resource allocation management for indoor power-line communications systems," *IEEE Transactions on Power Delivery*, vol. 22, no. 2, pp. 893–903, Apr. 2007.
- [46] N. Papandreou and T. Antonakopoulos, "Fair resource allocation with improved diversity performance for indoor power-line networks," *IEEE Transactions on Power Delivery*, vol. 22, no. 4, pp. 2575–2576, Oct. 2007.
- [47] T. N. Vo, K. Amis, T. Chonavel, and P. Siohan, "Achievable throughput optimization in OFDM systems in the presence of interference and its application to power line networks," *IEEE Transactions on Communications*, vol. 62, no. 5, pp. 1704–1715, May. 2014.
- [48] J. Shin and J. Jeong, "Improved outage probability of indoor PLC system for multiple users using resource allocation algorithms," *IEEE Transactions on Power Delivery*, vol. 28, no. 4, pp. 2228–2235, Oct. 2013.
- [49] Z. Xu, M. Zhai, and Y. Zhao, "Optimal resource allocation based on resource factor for power-line communication systems," *IEEE Transactions on Power Delivery*, vol. 25, no. 2, pp. 657–666, Apr. 2010.
- [50] F. Pancaldi, F. Gianaroli, and G. M. Vitetta, "Bit and power loading for narrowband indoor powerline communications," *IEEE Transactions on Communications*, vol. 64, no. 7, pp. 3052–3063, Jul. 2016.
- [51] T. F. do A. Nogueira, G. R. Colen, V. Fernandes, and M. V. Ribeiro, "Statistical modeling of magnitudes of brazilian in-home PLC and hybrid PLC-wireless channels," *Physical Communication*, vol. 39, p. 101014, Apr. 2020.
- [52] M. V. Ribeiro, G. R. Colen, F. V. p. De Campos, Z. Quan, and H. V. Poor, "Clustered-orthogonal frequency division multiplexing for power line communication: When is it beneficial?" *IET Communications*, vol. 8, no. 13, pp. 2336–2347, Sep. 2014.
- [53] A. Garg and A. K. Chaturvedi, "Generalization of hybrid time divisioning for power allocation in DMT-based DSL systems," *IEEE Communications Letters*, vol. 11, no. 6, pp. 504–506, Jun. 2007.



- [54] P. K. Pandey, M. Moonen, and L. Deneire, "Resource allocation in DMT transmitters with per-tone pulse shaping," in *IEEE International Conference on Acoustics, Speech and Signal Processing*, Mar. 2008, pp. 2777–2780.
- [55] S. Zhengguo, Z. Yijun, and Z. Yanyu, "The DMT-based bit-power allocation algorithms in the visible light communication," in *International Conference on Business Computing and Global Informatization*, Oct. 2012, pp. 572–575.
- [56] M. A. Tunç, E. Perrins, and L. Lampe, "Reduced complexity LPTV-aware bit loading for channel adaptation in broadband PLC," in *IEEE International Symposium on Power Line Communications and Its Applications*, Mar. 2012, pp. 206–211.
- [57] T. R. Oliveira, A. A. M. Picorone, S. L. Netto, and M. V. Ribeiro, "Characterization of brazilian in-home power line channels for data communication," *Electric Power Systems Research*, vol. 150, pp. 188 – 197, Sep. 2017.
- [58] A. Mukherjee, "Physical-layer security in the internet of things: Sensing and communication confidentiality under resource constraints," *Proceedings of the IEEE*, vol. 103, no. 10, pp. 1747–1761, Oct. 2015.
- [59] T. Park and W. Saad, "Distributed learning for low latency machine type communication in a massive internet of things," *IEEE Internet of Things Journal*, vol. 6, no. 3, pp. 5562–5576, Jun. 2019.
- [60] H. Seo, J. Hong, and W. Choi, "Low latency random access for sporadic MTC devices in internet of things," *IEEE Internet of Things Journal*, vol. 6, no. 3, pp. 5108–5118, Jun. 2019.
- [61] H. Yang, K. Zhang, K. Zheng, and Y. Qian, "Leveraging linear quadratic regulator cost and energy consumption for ultrareliable and low-latency IoT control systems," *IEEE Internet of Things Journal*, vol. 7, no. 9, pp. 8356–8371, Sep. 2020.
- [62] J. M. Cioffi, "Chapter 1: Discrete data transmission basics," accessed in November 2020. [Online]. Available: <http://cioffi-group.stanford.edu/doc/book/chap1.pdf>
- [63] C. C. Y. Dorea, C. R. Goncalves, and P. A. A. Resende, "Simulation results for Markov model selection: AIC, BIC and EDC," in *World Congress on Engineering and Computer Science*, vol. 2, Oct. 2014, pp. 899–901.
- [64] Â. Camponogara, T. R. Oliveira, R. Machado, W. A. Finamore, and M. V. Ribeiro, "Measurement and characterization of power lines of aircraft flight test instrumentation," *IEEE Transactions on Aerospace and Electronic Systems*, vol. 55, no. 3, pp. 1550–1560, Jun. 2019.
- [65] Tin Kam Ho, J. J. Hull, and S. N. Srihari, "Decision combination in multiple classifier systems," *IEEE Transactions on Pattern Analysis and Machine Intelligence*, vol. 16, no. 1, pp. 66–75, Jan. 1994.
- [66] P. Parada and R. Blahut, "Secrecy capacity of SIMO and slow fading channels," in *International Symposium on Information Theory*, Sep. 2005, pp. 2152–2155.
- [67] F. Oggier and B. Hassibi, "The secrecy capacity of the MIMO wiretap channel," *IEEE Transactions on Information Theory*, vol. 57, no. 8, pp. 4961–4972, Aug. 2011.

- [68] Â. Camponogara, H. V. Poor, and M. V. Ribeiro, “The complete and incomplete low-bit-rate hybrid PLC/wireless channel models: Physical layer security analyses,” *IEEE Internet of Things Journal*, vol. 6, no. 2, pp. 2760–2769, Apr. 2019.
- [69] Â. Camponogara, H. V. Poor, and M. V. Ribeiro, “Physical layer security of in-home PLC systems: Analysis based on a measurement campaign,” *IEEE Systems Journal*, pp. 1–12, Jun. 2020.
- [70] Â. Camponogara, H. V. Poor, and M. V. Ribeiro, “PLC systems under the presence of a malicious wireless communication device: Physical layer security analyses,” *IEEE Systems Journal*, vol. 14, no. 4, pp. 4901–4910, Dec. 2020.

## APPENDIX A – Publications

The conference paper published during the graduate period is as follows:

- Y. F. Coutinho, G. R. Colen, and M. V. Ribeiro, “An Enhanced Temporal Compressive Resource Allocation Technique for PLC Systems,” in *XXXVIII Simpósio Brasileiro de Telecomunicações*, Nov. 2020.

The journal paper submitted during the graduate period is as follows:

- Y. F. Coutinho, G. R. Colen, D. N. K. Jayakody, and M. V. Ribeiro, “The Lack of Transmission Power and Channel State Information Knowledge in the Finite Block Length Regime: A First Discussion,” *Digital Communications and Networks*, Mar. 2021.